University of Alberta
Department of Civil Engineering

Structural Engineering Report No. 80

Leakage Tests of Wall Segments of Reactor Containments

By

S.H. Rizkalla

S.H. Simmonds

and

J.G. MacGregor

October, 1979

LEAKAGE TESTS OF WALL SEGMENTS OF REACTOR CONTAINMENTS

by

S.H. Rizkalla

S.H. Simmonds

J.G. MacGregor

A technical report of the
Atomic Energy Control Board
Nuclear Plant Licensing Directorate
P.O. Box 1046
Ottawa, Ontario
Canada K1P 5S9

October 1979

DISCLAIMER

The interpretation of the technical data and any opinions or conclusions arising in this report are those of the authors only and do not necessarily reflect those of the cooperating agencies.

ABSTRACT

Two prestressed concrete wall segments simulating portions of containment walls were loaded by axial tensile forces to cause cracking of the concrete. At each load increment air pressure was applied in steps up to 21 psi to one side of the segment and the rate of leakage of air through the cracked concrete section was measured.

A theoretical equation for the flow of air through concrete cracks is developed and the results from one leakage test are used to determine the dimensionless constant required for this equation.

CONTENTS

LIST OF TABLES

LIST OF FIGURES

NOTATION

Symbols

A = BW	=	Cross section of flow path, ft^2.
B	=	extent of crack, ft.
C	=	coefficient
D	=	hydraulic diameter
E_c	=	modulus of elasticity of concrete at time of test
f'_c	=	compressive strength of concrete at time of test
f_t	=	split tensile strength of concrete at time of test
F	=	force
K	=	dimensionless constant
L	=	length of crack (distance through the wall), ft.
$\dot{m}$	=	mass flow rate, lb sec./ft.
p	=	pressure gradient
P	=	absolute air pressure at any section, $lb./ft.^2$
q	=	rate of flow through crack, $ft.^3/sec.$
Q	=	rate of flow through a group of cracks, $ft.^3/sec.$
R	=	gas constant
Re	=	Reynold's Number
T	=	absolute temperature, °K
V	=	air velocity at any section, ft./sec.
W	=	crack width, ft.
λ	=	dimensionless friction coefficient
μ	=	viscosity
ρ	=	mass air density, $lb. sec.^2/ft.^4$
τ_o	=	shear stress due to wall friction, $lb./ft.^2$

Subscripts

1 = beginning of crack

2 = end of crack

i = number of crack

CHAPTER I

1.1 INTRODUCTION

The nuclear reactors in Canadian nuclear power plants of the Gentilly-2 type are housed in circular prestressed concrete containment structures. Such a structure, shown schematically in Figure 1.1 consists of a heavy concrete base, a cylindrical wall, a ring beam and a spherical dome. Each element contains a grid of conventional reinforcement and prestressing tendons.

In the event of a malfunction, pressurized gases or steam may be discharged. The function of the secondary containment vessel is to prevent such gases from escaping into the atmosphere. The containment is designed to have zero tensile stress under 1.15 times the design basis accident (DBA) pressure of 18.5 psi which is the maximum pressure attained if a secondary steam line ruptures and the water dousing system acts to condense the steam.

In the extremely unlikely event that a secondary steam line fails and the dousing system also fails to act, internal pressures may reach several times the DBA pressure. This would result in the walls and dome of the containment being stressed in biaxial tension. The response of the containment structure to this overpressure is the purpose of a comprehensive study undertaken at the University of Alberta and for which this report is a part.

In order to obtain data on the response of the structural components to biaxial tension a series of 14 wall segments representative of construction details in the containment were tested. The relationship between a typical segment and the containment is shown in Figure 1.1.

Twelve of these were tested to obtain load-deflection and cracking behaviour of the structure. The results of these tests are given in Ref. 1.

This report describes the tests of the two wall segments which were tested to evaluate the rate of leakage through the containment wall after through cracking has occurred.

1.2 OBJECTIVE

The primary purpose of this report is to study the air leakage characteristics in thin walled prestressed containment structures. Specifically, the two main objectives of the wall segment tests are to investigate the relationship between the air leakage rate and concrete crack width, and to provide data for use in calibrating a mathematical expression for the leakage rate of compressed air escaping through cracked concrete.

1.3 SCOPE OF THIS REPORT

Two segments were tested under two different types of membrane loading. The first segment was prestressed and loaded in two directions, while the second was prestressed and loaded in one direction only. This report presents detailed information about these two segment tests, specimen properties, instrumentation, and data reduction.

Chapter 2 contains a description of the fabrication techniques used in constructing the segments. A discussion of the testing procedures and associated problems is given in Chapter 3. Chapter 4 discusses the preliminary formulation of the leakage problem and the assumptions that were used to relate the air leakage rate with the

concrete crack width. The test data is presented in Chapter 5 and a comparison between the test results and the derived mathematical expression is discussed in Chapter 6.

1.4 ACKNOWLEDGEMENTS

The research project "Study of Concrete Containment Structures Under Overpressure Conditions" was sponsored at the University of Alberta by the Atomic Energy Control Board of Canada and was under the general supervision of Dr. W.D. Smythe and Dr. F. Campbell of AECB. Principal investigators at the University of Alberta, Department of Civil Engineering, were Drs. J.G. MacGregor, D.W. Murray and S.H. Simmonds. Initially, Mr. Declan Whelan served as technical liaison between AECB and the project directors, however, since the summer of 1977, Dr. G.J.K. Asmis has served in this capacity.

The progress of the project has been reviewed from time to time by an Advisory Committee with representatives from the Atomic Energy Control Board, Atomic Energy of Canada Limited, Canatom Limited, Hydro Quebec and Ontario Hydro. The project directors wish to thank the members of this committee for the help and guidance received during this work.

Testing was carried out at the I.F. Morrison Structural Engineering Laboratory at the University of Alberta, Edmonton, Canada. Dr. S. Rizkalla was in charge of laboratory work.

CHAPTER II - TEST SPECIMENS

2.1 INTRODUCTION

Two wall segments were tested to obtain data on air leakage rate through walls of nuclear containment structures as shown in Figure 1.1. These two segments are part of a larger program of wall segment tests reported in Ref. 1 and are designated as segments 10 and 14. The overall dimensions and construction details of segments 10 and 14 corresponds to those of segments 1 and 5 respectively in that report. This report contains details of the construction and testing of segments 10 and 14.

2.2 DESCRIPTION OF THE SPECIMENS

The overall dimensions of the wall segments were 10.5" thick and 31.5" square. The first leakage specimen (segment 10) was post-tensioned with grouted tendons in the horizontal and vertical directions. The second specimen (segment 14) was prestressed only in the horizontal direction. The dimensions and reinforcement details for segment 10 are shown in Figure 2.1 and Figure 2.2. Segment 14 differs only by having the prestressing tendons in the three tendon direction.

In describing the specimens in the balance of the text, the word "face" will be used to refer to the 31.5 inch square sides. Face A is the surface that was on top when the specimen was cast and face B is the other side. The word "edges" will refer to the 10.5" by 31.5" sides through which reinforcement extends. During testing, the segment was positioned such that face A was towards the south. This permits references to the edges as the top, bottom, east or west edges.

The three tendons located at the mid-plane of the specimen represent the vertical tendons which are at the middle of the wall in the prototype. The four perpendicular tendons represent the circumferential tendons. In the prototype these are located near the outer quarter point of the wall thickness and due to the curvature of the wall, they produce a uniform compressive hoop stress through the wall thickness. In the wall segment, the center two of these tendons are placed adjacent to one face to simulate the actual cover and spacing of these tendons. The two remaining tendons are adjacent to the other face to maintain a uniform of prestress through the wall thickness. The properties of the two specimens are listed in Table 2.1.

2.3 CONSTRUCTION OF THE SPECIMENS

2.3.1 Segment 10

During the test two air chambers were provided, one on each face of the specimen. The upstream chamber was filled with pressurized air and the downstream chamber was used to collect the air that had leaked through the specimen.

To provide air proofing along the specimen edges so that the leakage would take place only from one face of the segment to the other, a rubber liner was placed around the edges of the specimen as shown in Figures 2.3 and 2.4. This liner also served as gasket for the connection of the chambers to the segment and served to eliminate any constraint from the chambers on the segment deformation during the test.

Placing of this rubber liner required a special construction sequence since the reinforcement bars and the prestressing tendons used

to provide the applied membrane loading protruded from the segment edges. The segment construction was as follows:

(1) The rubber liner was fabricated from 1/2" thick Neoprene sheet to form a square with inside dimension 31.5 in. Square corners were achieved by the rubber vulcanizing technique. Undersized holes to accommodate the reinforcement bars and bolts were punched as positioned in Figure 2.5 and Figure 2.6. These two figures show also the location of the square openings required for the prestressing tendons anchor heads. Extra holes were also provided for the lead wires from the embedded strain gauges.

(2) The rubber liner was placed inside a plywood form as shown in Figure 2.7. The liner was attached and kept in position by using 1/2" steel inserts distributed along the edges as shown in Figures 2.3 and 2.8.

(3) After the necessary electrical strain gauges had been attached to the rebars, the tendons and reinforcement were then placed in the form. The joint between the pipe in the end bearing plate and the tendon sheaths were sealed with a silicone rubber caulking compound to prevent concrete from leaking into the sheaths. Segment 10 is shown prior to casting in Figure 2.7.

(4) The concrete for a specimen was mixed in one 9 cu. ft. mix, approximately 6 cu. ft. being used in the specimen, the balance being used in test cylinders for tension and compression tests.

Internal vibrators were used to consolidate the concrete in the specimen with care being taken to avoid over-vibration

and bleeding. The specimen and cylinders were allowed to set and then were covered with wet burlap for 24 to 48 hours, after which time the forms were removed. The specimens and cylinders were then recovered with wet burlap and allowed to moist cure for one week. The curing continued in air until the specimens were prestressed.

(5) After removing the forms, the liner was secured to the concrete surface by means of bolts and washers screwed in the embedded steel inserts. These bolts and washers are clearly seen in Figure 2.4.

(6) Prestressing was carried out using a 100 kip center hole ram. The tendon was grouted with Master Flow 814 cable grout one or two days after the tendons were stressed. The age of the specimens when prestressed and tested are listed in Table 2.2.

2.3.2 Segment 14

Segment 10 was tested before Segment 14 was fabricated. During testing of Segment 10, considerable leakage was observed between the rubber liner and the edges of the segment in spite of the clamping action of the bolts and washers. To prevent these leakage problems for Segment 14, two rubber frames around the perimeter of the two faces of the segment were used in addition to the rubber liner. One end of the frames was joined to the liner and the free end was held in position by steel wires wrapped around the reinforcing bars. The concrete face was flared to be flush with the outer rubber surface. Details of the rubber frames and liner are shown in Figures 2.9 and 2.10. This liner proved to be entirely successful during testing.

The other construction details are identical to Segment 10. The age of the specimen when prestressed and tested is given in Table 2.2.

2.4 MATERIAL PROPERTIES

2.4.1 Concrete

The concrete used in the test specimens had the following nominal properties and composition for a 9 cu. ft. batch:

Design Strength	4500 psi
Water/cement ratio by weight	0.54
Water	113
Cement (Type Portland Cement)	208
Sand	423
3/8 in. gravel	560 lbs.

The gravel consisted of a glacial outwash gravel of quartzite, granites, etc.

Six 6 x 12 in. cylinders were cast with each specimen. The cylinders were cured in the lab in the same manner as the specimens. These were tested at the time of testing, three in compression and three as split cylinder tensile tests. The results are summarized in Table 2.2.

2.4.2 Reinforcing Steel

The reinforcement used in these tests consisted of hot rolled deformed bars conforming to CSA G30.12-72. No. 3 bars were used, all

bars coming from the same heat. Four specimens were tested in tension and had the following average strengths and moduli of elasticity:

Yield strength, ksi	58.2
Ultimate Tensile Strength, ksi	87.5
Modulus of Elasticity, 10^3 ksi	28.9

2.4.3 Prestressing Tendons

The prestressing tendons consisted of six or seven individual straight, smooth 0.276 in. diameter wires and were supplied as a pre-assembled unit containing bearing plates and flexible metal sheath as shown in Fig. 2.11. The tendons in the four tendon direction had seven wires each. The stress-strain properties of the tendons, based on mill test results provided by the wire manufacturer and a tension test of a tendon, are yield strength (stress at 1% strain) 236 ksi, ultimate tensile strength of 264 ksi and modulus of elasticity of 29,200 ksi.

The tendon assemblies were specially manufactured for this project by Canadian BBR Ltd. This system was chosen since BBR tendons were used in the Gentilly-2 containment structure.

2.5 PRESTRESSING FORCE

During prestressing and during the period until the tendons were grouted the prestress force was measured using load cells made from hollow aluminum cylinders split in two pieces to fit around the tendon. Descriptions are given in detail in Reference 1. After grouting, the load cells were filled with grout and the tendons were bonded to the concrete, hence further load cell readings were meaningless.

Due to the small size of the specimens the measurements used

to evaluate the prestress losses were unreliable. A computer program was written to calculate the losses based on the measured strength of the concrete, creep and shrinkage data obtained earlier for similar concretes and relaxation data for the wire used. Based on the results of the computer analyses and the measurements made prior to grouting, the losses were assumed to be 12 percent in the four tendon direction and 8 percent in the three tendon direction for all specimens.

CHAPTER III - TESTING PROGRAM

3.1 INTRODUCTION

When a nuclear containment structure is subjected to high internal overpressure, the membrane stresses will exceed the cracking strength of concrete resulting ultimately in cracks passing through the wall. At this point, leakage through the wall will take place if the containment is not lined.

In the containment structure, the magnitude of the membrane stresses, and hence the crack width, is a function of the internal pressure. In the leakage segment test, the situation is simulated by applying tensile membrane forces to the reinforcing bars protruding along the edges of the specimen and providing an air pressure to the upstream face of the segment. The tensile forces applied to the segment are independent of the applied air pressure. In this way, the load-pressure ratio of the segment need not correspond directly with that in the containment wall. The maximum air pressure that could be applied to the segment face is restricted only by the ability to prevent leakage and the strength of the pressure chambers. For a given tensile force and hence crack width, it is possible to vary the air pressure in the upstream face of the segment. This permits an evaluation of the leakage rate for different pressure levels through a given crack width.

By obtaining leakage rates for a series of air pressures for increasing crack width, the predicted capacity of the theoretical formulation of leakage rate can be verified.

3.2 APPLIED MEMBRANE FORCES

In the walls of a containment structure, the internal pressure loading will induce circumferential stresses in the wall σ_1 which are twice the longitudinal stresses, σ_2, see Figure 1.1(a). In the prototype structure, these are offset by prestressing forces which are larger in the circumferential direction. Segment 10 was prestressed and loaded to represent this condition.

Segment 14 was prestressed and loaded in one direction only. This permits verifying the leakage theory for the uniaxial condition.

Loads were applied to the segments through reinforcing bars and prestressing tendons, which protruded beyond the edges of the segment, through a series of yokes and pulling rods. The loading apparatus employed for Segment 10 consisted of a 1,400,000 lb. capacity MTS universal testing machine to apply the "circumferential" load to the specimen and a specially designed load frame and four 200 kips hydraulic rams to apply the "longitudinal" load to the specimen. In the tests, the segment is turned through 90 degrees so that the circumferential load (horizontal in the prototype) is applied vertically in the laboratory as shown in Figure 1.1(b). This is done to make use of the large capacity of the MTS machine to apply the larger of the two loads. A photograph of one end of the load frame is shown in Figure 3.1 and cross sections through the frame are shown as Figures 3.2 and 3.3. Detail of these fittings including the loading frame are reported in Reference (1).

The vertical load increments were controlled by the MTS electro-hydraulic loading rate controllers. The horizontal loads were applied simultaneously by hydraulic tension rams controlled by a manually

operated console which used air pressure to activate the hydraulic fluid.

In general the loading procedure for Segment 10 followed those of the non-leakage segments. A more detailed description of the loading procedure is given in Reference (1).

Membrane force was applied to Segment 14 only in the "longitudinal" direction and hence only the load from the load frame and four hydraulic rams was required. This permitted this segment to be tested outside of the MTS testing machine.

3.3 APPLIED AIR PRESSURE

An air rigid chamber was placed on each face of the specimen. These chambers were formed with aluminum channels and covered by 1 inch plexi-glass to permit observation of the concrete surface and mapping the crack pattern. The two chambers were bolted to the rubber liner as shown in Fig. 2.3.

The upstream chamber was pressured by an air-compressor through a pressure regulator which controled the pressure inside the chamber. This chamber was designed to maintain an internal air pressure of 25 psi and it was braced from inside to reduce the deformation and stresses on the plexi-glass, Figure 3.4. The upstream chamber was adjacent to Face A of the specimen.

The downstream chamber shown in Figure 3.5 was connected to a measurement device to measure the air leakage through the concrete. No bracing was needed since the internal pressure in the chamber was kept atmospheric. A section through the leakage chambers and specimen is shown in Fig. 2.3.

3.4 INSTRUMENTATION

Approximately 62 items were recorded at each load level, including loads, strains, air pressure, temperature and leakage rate. The different measuring devices and data obtained can be briefly summarized as follows:

1. Vertical Applied Membrane Load - The load was applied by a 1,400,000 lb. capacity MTS Universal testing machine and measured by differential pressure transducers.
2. Horizontal Applied Membrane Load - A specially designed frame and four 200 kips hydraulic rams were used to apply the horizontal load. The load was measured by electric resistance strain gauges mounted on clevices between the hydraulic rams and end fittings.
3. Air Leakage - The rate of flow was evaluated by measuring the total volume of air leaving the downstream chamber within a certain specified time interval. For both segments the volume of air was measured using an American Dry Test Meter, Model DTM-115-3 which could be read to 0.001 L. The time was measured with a stop watch. The volume over three separate one minute intervals was obtained for each load increment from which the average leakage rate was computed.

   For Segment 10 the rate of flow was also measured using a Rotameter as supplied by Matheson of Canada Ltd. This meter consists of two spherical metering floats, one of glass and one of stainless steel, and is calibrated to give the rate of flow directly. This device was not used for Segment 14 since it was found that it built up a significant pressure on the

downstream side and was only reliable in the lower range of air leakage.

4. Forces Transferred to Tendons - Measured by electric resistance strain gauges mounted on pull rods between end fittings and specimens. These gauges are indicated by numbers 37 to 50 in Figure 3.6.

5. Forces Transferred to Reinforcement - Measured by electric resistance strain gauges mounted on six reinforcing bars between the specimen and the end fittings on each edge of the specimen. These gauges are indicated by numbers 13 to 36 in Figure 3.7.

6. Reinforcement Strains - Measured by twelve electric resistance strain gauges mounted on the reinforcing bars and embedded in the concrete as shown in Figures 3.7 and 3.8 for Segments 10 and 14, respectively. These gauges are indicated by numbers 1 to 12 in Figure 3.6.

7. Elongation - Measured by LVDT extensometers resting on the edges of the specimen.

The steel strain gauges were electric wire resistance strain gauges, 0.25 in. in length, 0.125 in. in width, and 120 ± .15% ohm resistance. The electric resistance strain gauges and MTS load values were read directly by the laboratory data acquisition system. Other readings were read and recorded manually. Further details on the instrumentation and data reduction are given in Reference 1.

3.5 DATA ACQUISITION SYSTEM

Wherever possible, data was read and recorded using the data acquisition system in the laboratory which includes as control unit, a Nova 210/E digital computer. This unit can receive and process the input from up to 254 channels, has a central processor core size of 32K words and a dual disk drive system (Reference 1).

3.6 TEST PROCEDURE

A typical test of a wall segment required roughly 6 days to set up the specimen in the test frame, one day to run and one day to dismantle. The set up process included placing and aligning the specimen in the testing machine and load frame, attaching the instrumentation, and connecting the tendon pull rods and reinforcing bars. During this process the specimen was loaded to roughly one-third the cracking load and unloaded a number of times with adjustments being made each time to the tendon pull rods until the force transferred to each tendon was approximately equal. Following this, angles welded to the reinforcing bars were bolted to the end-fittings. The specimen was loaded a number of times with adjustments being made each time to the angle until the force was equally taken by the rebars.

During the test the horizontal loads were manually controlled, care being taken to apply load at an even rate and to prevent horizontal displacement of the specimen due to uneven rates of loading at the two ends. The vertical loads were either manually controlled to be the correct multiple of the horizontal load currently on the specimen or were controlled by presetting the rate of loading adjustment on the machine.

The magnitude of the membrane load was held constant during measurement intervals except that during the last two intervals prior to the end of the test the deformation was held constant during the measurements. While the load was held constant, the pressure in the upstream chamber was increased in increments of 2.5 psi, while the pressure in the downstream chamber of the specimen was kept at atmospheric. For each increment, the rotameter and three readings of the dry test meter were recorded to evaluate an average value for the rate of leakage. The maximum pressure that could be maintained for Segment 10 was 10 psi. By using the new improved rubber liner, the pressure was increased up to 21 psi for Segment 14. The test for each segment took about 10 hours with each load level requiring about 50-60 minutes. The majority of this time was spent in reading the air leakage meters.

Testing was terminated when the maximum tendon forces reached 95 to 98 percent of the breaking strength of the tendons. This was done to avoid damage to the instrumentation on the tendon pull rods.

CHAPTER IV - MATHEMATICAL FORMULATION FOR LEAKAGE RATE

4.1 INTRODUCTION

When a reinforced concrete section is loaded in biaxial tension a family of parallel cracks will occur in each direction. The width of these cracks will vary according to a statistical distribution which is a function of the amount of reinforcement among other things. In general the geometrical configuration of a particular crack extending through the section is extremely complex. Thus it is almost impossible to model accurately the path of a particular crack and since each crack is unique, modelling accurately any particular crack would be of limited application. Hence some idealization of the crack geometry is necessary.

In the absence of bending moment, the width of any given crack should be reasonably uniform through the thickness. Therefore the assumption is made that for membrane loading, the width of any given crack may be considered constant along its length.

The development of a procedure to predict leakage through cracked concrete sections begins with a review of the derivation of fluid flow through an idealized crack. This theoretical treatment for a single crack is then extended for multiple cracks of different widths. The flow constants from the segment tests are then evaluated in Chapter 6.

4.2 MOMENTUM BALANCE FORMULATION

The mathematical formulation of the flow of compressible gas through a duct of constant cross-section using the concept of momentum balance has been presented (2). In this derivation the air flow is

assumed to be adiabatic and the friction coefficient factor is constant along the length of the flow path.

The essential principle is that the mass flow rate, $\dot{m}$, will remain unchanged along the flow path. This quantity can be expressed in terms of the physical quantities

$$\dot{m} = \rho AV = \text{constant} \tag{4.1}$$

where ρ = mass air density, lb. sec.^{2}/ft.^{4}

A = cross section of flow path, ft.^{2}

V = air velocity at any section, ft./sec.

If the flow through a concrete crack is idealized as the flow through the gap between two parallel plates as shown in Fig. 4.1 then from the momentum-impulse theorem which states that the sum of the forces equals the change in momentum:

$$\Sigma F = \text{change in momentum}$$

$$PA - (P + dP)A - 2\tau_o \, Bdx = \rho AV(V + dV) - \rho AV(V)$$

or
$$dP + \rho V dV + 2\tau_o \frac{B}{A} dx = 0 \tag{4.2}$$

where P = absolute air pressure at any section, lb./ft.^{2}

A = BW, ft.^{2}

B = extent of crack (see Fig. 4.1), ft.

W = crack width = gap between parallel plates, ft.

τ_o = shear stress due to wall friction, lb./ft.^{2}

In steady, uniform, turbulent flow in conduits of constant cross section, the wall shear stress has been expressed in terms of the velocity as

$$\tau_o = \frac{\lambda}{4} \frac{\rho V^2}{2}$$

where λ is a dimensionless friction coefficient factor. Substituting expressions for τ_o and A into (4.2) one obtains

$$dP + \rho V dV + 2 \frac{\lambda}{4} \frac{\rho V^2}{2} \frac{B dx}{BW} = 0$$

which when divided by ρV^2 yields

$$\frac{dP}{\rho V^2} + \frac{dV}{V} + \frac{\lambda}{4W} dx = 0 \qquad (4.3)$$

From the perfect gas law

$$P = \rho RT \qquad (4.4)$$

where R = gas constant

T = absolute temperature

From Eqns. (4.1) and (4.4)

$$V^2 = \frac{\dot{m}^2}{\rho^2 A^2} ; \qquad \rho = \frac{P}{RT}$$

hence

$$\rho V^2 = \frac{\dot{m}^2 RT}{A^2 P}$$

Substitution of this expression into Eqn. (4.3) gives

$$\frac{A^2}{\dot{m}^2 RT} PdP + \frac{dV}{V} + \frac{\lambda}{4W} dx = 0 \qquad (4.5)$$

Eqn. (4.5) can be integrated along the length of the crack, L, (distance through the wall) giving:

$$\frac{A^2}{\dot{m}^2 RT} \frac{P_2^2 - P_1^2}{2} + \ell n \left(\frac{V_2}{V_1}\right) + \frac{\lambda}{4W} L = 0 \qquad (4.6)$$

where subscript 1 represents conditions at the beginning of the crack and subscript 2 at the end of the crack.

Since $\dot{m}$ is constant along the crack

$$\dot{m}_1 = \dot{m}_2$$

$$\rho_1 A V_1 = \rho_2 A V_2$$

$$\frac{P_1}{RT} A V_1 = \frac{P_2}{RT} A V_2$$

hence $$\frac{V_2}{V_1} = \frac{P_1}{P_2}$$

Substitution into Eqn. 4.6 yields

$$P_1^2 - P_2^2 = \frac{\dot{m}^2 RT}{A^2} \left[2 \ln \left(\frac{P_1}{P_2}\right) + \frac{\lambda L}{2W}\right] \tag{4.7}$$

Let q = rate of flow through crack, ft.^{3}/sec.

$= V_1 A$

The coefficient can be written as

$$\frac{\dot{m}^2 RT}{A^2} = \frac{P_1^2 A^2 V_1^2 RT}{A^2} = \frac{P_1^2}{RT} \frac{q^2}{B^2 W^2}$$

Substitution into Eqn. (4.7)

$$P_1^2 - P_2^2 = \frac{P_1^2}{RT} \frac{q^2}{B^2 W^2} \left[2 \ln \left(\frac{P_1}{P_2}\right) + \frac{\lambda L}{2W}\right]$$

This can be rewritten as

$$P_1^2 - P_2^2 = \frac{\lambda L}{2} \frac{P_1^2}{RT} \frac{q^2}{B^2 W^2} \left[\frac{4W}{\lambda L} \ln \left(\frac{P_1}{P_2}\right) + 1\right]$$

The first term in the bracket is always very small compared to unity and can be neglected. Hence:

$$P_1^2 - P_2^2 = \frac{\lambda L}{2} \frac{P_1^2}{RT} \frac{q^2}{B^2 W^2} \tag{4.8}$$

The friction factor λ is a function of the velocity V, hydraulic diameter D, density, ρ, viscosity μ, and certain characteristics of the wall roughness which are represented by the dimensionless constant K. Introducing Reynolds number, Re, to obtain a dimensionless expression for λ, one obtains

$$\lambda = \frac{K}{Re} = \frac{K\mu}{\rho_1 V_1 D}$$

The hydraulic diameter is defined as four times the cross section divided by the wetted perimeter. For flow through a crack this is 4BW/2(B + W) which can be approximately closed as 2W.

Hence $$\lambda = K\mu\left(\frac{RT}{P_1}\right)\left(\frac{A}{q}\right)\frac{1}{2W} = \frac{K\mu RTB}{2P_1 qW}$$

Substituting this expression for λ in Eqn. (4.8) yields

$$P_1^2 - P_2^2 = \frac{K\mu L P_1 q}{4BW^3}$$

Dividing by P_1

$$\frac{P_1^2 - P_2^2}{P_1} = \frac{K\mu L}{4B}\frac{q}{W^3} \qquad (4.9)$$

Introducing expressions

$$p = \frac{P_1^2 - P_1^2}{P_1} \quad \text{and} \quad C = \frac{K\mu L}{4B}$$

where p is referred to as the "pressure gradient", Eqn. (4.9) can be written as

$$p = C\frac{q}{W^3} \qquad (4.10)$$

4.3 PRESSURE DECREASE COEFFICIENT FORMULATION

Eqn. (4.10) can also be obtained using the procedure outlined by Buss for the analysis of air flow through concrete cracks (3). He relates the rate of pressure decrease through the crack to the friction coefficient by the expression

$$-\frac{d\rho}{dx} = \frac{\lambda}{D}\frac{\rho V^2}{2} \tag{4.11}$$

Again using the principle that the mass flow rate, $\dot{m}$ is constant and the perfect gas law

$$V = \frac{P_1}{\rho} V_1$$

Substituting into Eqn. (4.11) and integrating

$$-\int_{P_1}^{P_2} PdP = \frac{\lambda}{D}\frac{\rho_1 V_1^2}{2} P_1 \int_o^L dx$$

or

$$\frac{P_1^2 - P_2^2}{P_1} = \frac{\lambda L \rho_1 V_1^2}{D} \tag{4.12}$$

Introducing $\lambda = \frac{K}{Re}$, Eqn. (4.12) can be made identical to Eqn. (4.10)

4.4 LEAKAGE RATE FOR MULTIPLE CRACKS

Eqn. (4.10) relates the flow rate, q, for a simple crack of width W length L and extending a distance B for a given pressure gradient p. When applied to a surface having many cracks each having a different width and length the total flow rate Q is merely the sum of

the flow rates through the individual cracks. Hence if there are j cracks,

$$Q = \sum_{i=1}^{j} q_i$$

which using Eq. (4.10) can be written as

$$Q = p \sum_{i=1}^{j} \frac{W_i^3}{C_i}$$

$$Q = p \frac{4}{K\mu} \sum_{i=1}^{j} \frac{B_i W_i^3}{L_i} \qquad (4.13)$$

The constant K must be determined from experimental data. Eqn. (4.13) can then be used to determine the flow rate through a concrete section having multiple cracks of known geometry.

CHAPTER V - TEST RESULTS

5.1 INTRODUCTION

This chapter will review the test results for the two leakage specimens and summarize the test findings. A listing of all readings taken for Segments 10 and 14 are given in Appendix A.

5.2 FIRST LEAKAGE SPECIMEN (SEGMENT 10)

The properties of Segment 10 are summarized in Table 5.1 and correspond to those for comparison Segments 1 and 2 in Reference (1). The ratio of the applied membrane load was 2:1 with the larger load applied in the vertical (i.e. 4 tendons) direction. Loads were increased in increments of 50 kips vertically and 25 kips horizontally. At each increment an air pressure was applied to the upstream face in increments of 2.5 psi. During the first portion of testing, the largest pressure that could be maintained in the upstream chamber was 10 psi, however, at later stages of the test, due to leakage of the air-proofing system, the maximum pressure that could be maintained was only 5 psi.

Although the exposed surface (Face A) was kept moist during the initial curing period, a few shrinkage cracks were observed near the location of some of the reinforcement. Similar cracks were also observed in the other segments reported in Reference (1).

Up to a load of 300 kips in the vertical direction there were no signs of cracking due to applied load and no leakage through the specimen was measured.

The first cracks due to applied load were observed at a vertical load of 350 kips. These were horizontal cracks and occurred

both at and between existing shrinkage cracks. No new vertical cracks were observed. The first measurable air leakage occurred at this loading. For each pressure increment, three leakage rate readings were recorded to obtain an average value of air leakage rate.

Due to the problems of sealing the edges of the segment and the variable back pressure later observed when using the rotameter the leakage measurements were somewhat erratic at higher flow rates. For this reason, the leakage measurements for segment 10 were not processed further.

The first vertical cracks due to load were observed when the horizontal load was 187 kips (vertical = 375 kips). Although this was not a normal load increment, a set of air pressure leakage readings were taken. Another set was taken at the usual increment (i.e. horizontal load = 200 kips). Photographs of both sides of this specimen after testing are given in Figures 5.1 and 5.2 from which the crack pattern can be observed. It should be noted that the cracks were marked after the specimen had been unloaded and cracks which had closed may have been missed. In general, the overall behaviour of this specimen was similar to the corresponding specimens with regard to crack sequences and load-stress response.

The load-strain curve for each embedded steel strain gauge in both vertical and horizontal directions are given in Figs. 5.3 to 5.6. In general the strains from similar gauges agree closely even in the post-cracking region. The average strains in both directions are plotted versus load in Fig. 5.7. From these plots the cracking load and load at yielding of the reinforcement can be obtained.

To compare the average strains in Segment 10 with those obtained from corresponding Segments 1 and 2, Figs. 5.8 and 5.9 were plotted. It is seen that in the pre-cracking region agreement is excellent. Due to the lower tensile strength in Segment 10, however, the first cracking occurred at a lower load, although the stiffness after cracking was similar.

5.3 SECOND LEAKAGE SPECIMEN (SEGMENT 14)

The properties of Segment 14 are summarized in Table 5.2 and correspond to those of Segment 5 reported in Reference (1). The applied membrane load was in the horizontal direction only (i.e. in the three tendon direction). Loads were increased in increments of 25 kips. At each increment air pressure was applied to the upstream face of the specimen (Face A) in increments of 2.5 psi up to 20 psi, with one additional increment at 21.0 psi which roughly represents a pressure difference of 1.5 times the absolute atmospheric pressure. The modified air-proofing rubber liner described in Section 2.3.2 was able to maintain this high air pressure without problems during the course of the test. However, at later stages of the test, the maximum pressure that could be maintained was only 15.0 and 10.0 psi for load levels of 350 and 375 kips, respectively, due to an insufficient supply of air volume. At the final load of 400 kips, the leakage rate was sufficiently large that only 3.75 psi would be maintained.

Up to the load of 200 kips, there were no signs of cracks due to the applied load and no measurable leakage through the specimen was observed.

The first cracks due to the applied load were observed at a horizontal load of 225 kips. For each pressure increment, three leakage rates were recorded to obtain an average value of air leakage rate. Table 5.3 summarizes the air leakage measurements at the different load increments. Photographs of both sides of the segment after testing are given in Figures 5.10 and 5.11. Again, these cracking patterns were observed after the specimen had been unloaded and cracks which had closed may not have been marked. The specimen behaviour was similar to Segment 5 reported in Reference (1).

The load-strain curve for each embedded steel strain gauge in the direction in which the load was applied are given in Figs. 5.12 and 5.13. The agreement between individual gauges is very close prior to final cracking and the stiffness in the post-cracking region is similar. The load-average strain curve based on the six embedded steel strain gauges is given in Fig. 5.14 and is compared to a similar curve for Segment 5 in Fig. 5.15.

CHAPTER VI - LEAKAGE THROUGH CONCRETE SECTIONS

6.1 PROPOSED METHODOLOGY FOR PREDICTING FLOW RATE

Eqn. (4.13) gives an expression that was determined theoretically for the rate of flow through a series of idealized cracks. In order to use this expression it is necessary to know the width and extent of each individual crack. This approach is not practical when attempting to predict leakage through wall segments of concrete containment structures since the width of individual cracks is unknown. To extend the theoretical formulation to concrete segments under biaxial tension involved the following reasoning.

The length of all cracks, L is taken as the wall thickness and hence for any wall segment will be constant. This permits L_i to be taken outside the summation sign. Similarly, at advanced stages of cracking, all through-the-wall cracks will extend across the segment and B_i may also be considered as known and constant for a given loading. This permits rewriting Eqn. (4.13) as

$$Q = p \frac{4}{K\mu} \frac{B}{L} \sum_{i=1}^{j} W_i^3 \qquad (6.1)$$

$$= \frac{p}{C} \sum_{i=1}^{j} W_i^3$$

where $C = \frac{K\mu L}{4B}$

To eliminate the need to consider widths of individual cracks the concept of an equivalent crack width, W, is introduced. The width of this equivalent crack is representative of the statistical distri-

bution of crack widths for a particular cross section and for this study is taken as the mean value of the measured cracks. The prediction of the mean crack width for various cross sections will be discussed in a subsequent report (4).

This concept permits replacing the summation with an exponential function of the equivalent crack width.

$$W^n = \sum_{i=1}^{j} W_i^3 \tag{6.2}$$

The value of the exponent n must be evaluated from tests but regardless of the value, W^n will be a constant at a given load level. Eqn. (6.1) can now be written

$$Q = \frac{p}{C} W^n \tag{6.3}$$

or

$$p = \frac{C}{W^n} Q = DQ \tag{6.4}$$

To verify the above reasoning a plot of p vs. Q should result in a straight line, the slope of which is the value of the constant D which relates the flow rate to the pressure gradient for a given equivalent crack width W, which in turn depends on the level of applied load.

Such a plot is given in Fig. 6.1. The data shown is for Segment 14. Due to problems with sealing the perimeter of Segment 10 the results were not used. It is seen from Fig. 6.1 that there is a reasonably linear relationship between pressure gradient and flow rate for all load levels. Value of D obtained from a linear regression of the data points for each load are given in Table 6.2. The data for load level P = 375^k has not been included since no measurement could be made

at the higher air pressures.

The constant of proportionality, D, at any given load and hence crack width can be expressed as

$$\ell nD = \ell nC - n\ell nW \qquad (6.5)$$

A plot of this equation on log-log paper should result in a straight line, the slope of which is the exponent n. Such a plot for Segment 14 is given in Fig. 6.2. The crack widths used are the mean values of crack widths measured from corresponding Segment 5 and are given in Table 6.2. It can be seen that at only four load levels are there values of D in Table 6.2 and crack widths in Table 6.1. The plot is linear and has a slope equal to 3. The linear plot verifies the concept of replacing a statistical population of crack widths with an equivalent crack width equal to the mean, and the slope of the line indicates that the power of the equivalent crack width is the same as for the individual cracks.

The constant, C can be evaluated from Eqn. (6.4) for any load level, m

$$C = D_m W_m^3$$

Values of C corresponding to the four load levels at which values of both D and W are available are given in Table 6.2. The average value of C is 1.86×10^{-6} lb. sec./ft.^{2}.

This permits an evaluation of the constant K which relates the friction coefficient factor to Reynolds number. The expression for K is

$$K = \frac{4BC}{\mu L}$$

For Segment 14 the total length of cracking B was measured as 11.9 ft. This was the average of the lengths on the two faces. The length, L, is equal to the segment thickness or 0.875 ft. At 70°F the viscosity of air is 0.38×10^{-6} lb. sec./ft.^{2}. For these values K computes as 267.

K is the dimensionless constant which is a measure of the wall roughness and hence may be considered constant for all concrete cracks. Using the value of K obtained from the test permits evaluating C for any specified crack pattern, i.e. values of B and L. With this computed value of C, Eqn. 6.3 can be used to compute the flow rate through concrete cracks for any given, pressure gradients, q, and equivalent crack width, W.

6.2 RELIABILITY OF TEST RESULTS

The value of K, the dimensionless constant that relates the friction coefficient factor to Reynolds number obtained in this study was 267. The reliability of the proposed methodology and test results may be evaluated by comparing this value with published results.

From purely theoretical considerations the value of K for flow through circular tubes is 64 (2) and for flow between parallel plates is 96 (3). Buss (3) also conducted a series of flow measurements through induced cracks in slab sections. From these tests he obtained values of K ranging from 400 to 2000 with a mean value of 1200. Direct comparison is difficult since his test specimens had a simple crack with signficantly larger induced crack width than those occurring in the segments tested in this study.

The value of 267 for K was computed on very limited test data. Due to air-proofing problems with Segment 10 only the leakage results obtained from Segment 14 were used. The effective crack widths were obtained from the corresponding specimen, Segment 5. While the load-strain response for these two segments as obtained from embedded steel strain gauges was in close agreement there is no way of verifying that the crack widths also agreed closely although the crack widths are strongly related to gross strain.

Readings of flow rates from Segment 14 correspond to recorded crack widths from Segment 5 at only four levels of load. The value of K is based on these four sets of readings. In addition, this value was obtained for uniaxial load only and may not be the same for biaxial loading.

While the accuracy of the value of K may be in some doubt due to the limited experimental data, the linearity of the plots for Segment 14 tends to verify the validity of the proposed methodology for predicting leakage through concrete sections having many cracks of variable widths. To obtain an estimate of the reliability of the predicted leakage rates would require a much more extensive testing program.

6.3 RECOMMENDATIONS FOR FUTURE TESTS

Should further testing be undertaken, the following items should be considered.

1. The crack widths and leakage flow rates should be measured on the same segment at smaller increments of applied load.
2. A sufficiently large pressure difference between the two faces should be applied to determine possible effects of transfer from laminar to supersonic flow.

3. Segments loaded in both biaxial tension and bending should be included to study effects of leakage in regions of membrane stress and moment gradient in the containment structure.
4. For at least one set of variables there should be sufficient replication of tests to obtain a statistical scatter to permit some evaluation of the expected level of confidence in the predicted flow rates.

REFERENCES

1. Simmonds, S.H.; Rizkalla, S.H. and MacGregor, J.G., "Tests of Wall Segments from Reactor Containments," Structural Engineering Report No. 81, Department of Civil Engineering, University of Alberta, October 1979.

2. John, J.E.A., "Gas Dynamics," Allyn and Bacon, Boston, 1969, 394 pp.

3. Buss, W., "Proof of Leakage Rate of a Concrete Reactor Building," Paper 34-61, Concrete for Nuclear Reactors, ACI Special Publication SP-34, Vol. III, 1972, pp. 1291-1320.

4. MacGregor, J.G.; Rizkalla, S.H. and Simmonds, S.H., "Cracking of Reinforced and Prestressed Concrete Wall Segments," Structural Engineering Report No. 82, Department of Civil Engineering, University of Alberta, October 1979.

TABLE 2.1

SPECIMEN PROPERTIES

SEGMENT*	PRESTRESSED	NON-PRESTRESSED REINFORCEMENT**	MIN. CONC. COVER IN.	LOADING RATIO H/V	THICKNESS IN.	REMARKS
10	two	10 # 3 @ 3 in.	0.5	1:2	10.5	
14	one	10 #3 @ 3 in.	0.5	1:0	10.5	Loaded in three tendon direction only, other tendons omitted.

* The numbering system in this report corresponds to that in Ref. 1.

** Each face of the specimen had one such layer in each direction.

TABLE 2.2

MATERIAL PROPERTIES OF CONCRETE

SPECIMEN	AGE AT PRESTRESSING, DAYS	AGE AT TEST DAY	COMPRESSIVE STRENGTH, PSI	SPLIT TENSILE STRENGTH, PSI	MODULUS OF ELASTICITY 10^3 KSI (FROM CYLINDER TEST)	$f_t/\sqrt{f'_c}$	$E_c/\sqrt{f'_c}$
10	57	158	3770	400	3.24	6.51	52.7
14	35	77	3970	423	2.83	2.71	44.9

TABLE 5.1

PROPERTIES OF SPECIMEN 10

Loading Ratio (Vertical, Horizontal) = 2:1

CONCRETE

Strength

Compression = 3770 psi

Tension = 400 psi

REINFORCEMENT

Pattern - 10 #3 @ 3 in each way

Yield Strength = 58.2 ksi

PRESTRESSING FORCE

Vertical (Four 7 wire tendons) = 64 kips/tendon

Horizontal (Three 6 wire tendons) = 48.1 kips/tendon

CRACKING LOAD

Horizontal Cracks = 350 kips

Vertical Cracks = 187 kips

TABLE 5.2

PROPERTIES OF SPECIMEN 14

Loading Ratio (Vertical, Horizontal) = 0:1

CONCRETE

Strength

Compression = 3970 psi

Tension = 423 psi

REINFORCEMENT

Pattern - 10 #3 @ 3 in each way

Yield Strength = 58.2 ksi

PRESTRESSING FORCE

Horizontal (Three 7 wire tendons) = 48.1 kips

CRACKING LOAD

Vertical Cracks = 225 kips

TABLE 5.3

AIR FLOW RATE OF SEGMENT 14 - Q FT.^{3}/SEC. x 10^{-3}

APPLIED LOAD (kips)	APPLIED AIR PRESSURE (psi)								
	2.5	5	7.5	10	12.5	15	17.5	20	21
225	0	0	0.962	2.094	3.473	4.778	6.632	8.545	9.476
250	2.354	5.65	9.506	14.98	20.6	25.43	32.37	38.85	42.38
275	7.024	14.71	22.72	30.9	40.02	50.32	59.74	70.042	76.52
300	12.24	24.13	36.61	48.85	61.8	75.93	88.87	101.23	106.53
325	18.25	34.73	50.32	69.45	87.69	105.35	125.66	141.26	153.03
350	30.02	61.21	92.70	120.07	160.39	203.06			
375	72.39	126.54	183.64	223.07					
400	174.81	214.23 @ 3.75 psi							

TABLE 6.1

EQUIVALENT CRACK WIDTH FOR LEAKAGE ANALYSIS
FOR SPECIMEN NO. 14

LOAD (kips)	CRACK (in.)
225	-
250	-
275	0.0032
300	0.0040
375	0.0043
350	0.0053
375	0.0055

TABLE 6.2

VALUES OF D AND C
MEASURED IN TEST OF SPECIMEN 14

LOAD INCREMENT KIPS	AVERAGE CRACK WIDTH (in.)	D lbf • sec./ft.^{5}	$C_i = D_i W_i^3$ lbf • sec./f^2
275	0.0032	86400	1.638×10^{-6}
300	0.004	50400	1.866×10^{-6}
375	0.0043	37440	1.723×10^{-6}
350	0.0053	25920	2.233×10^{-6}

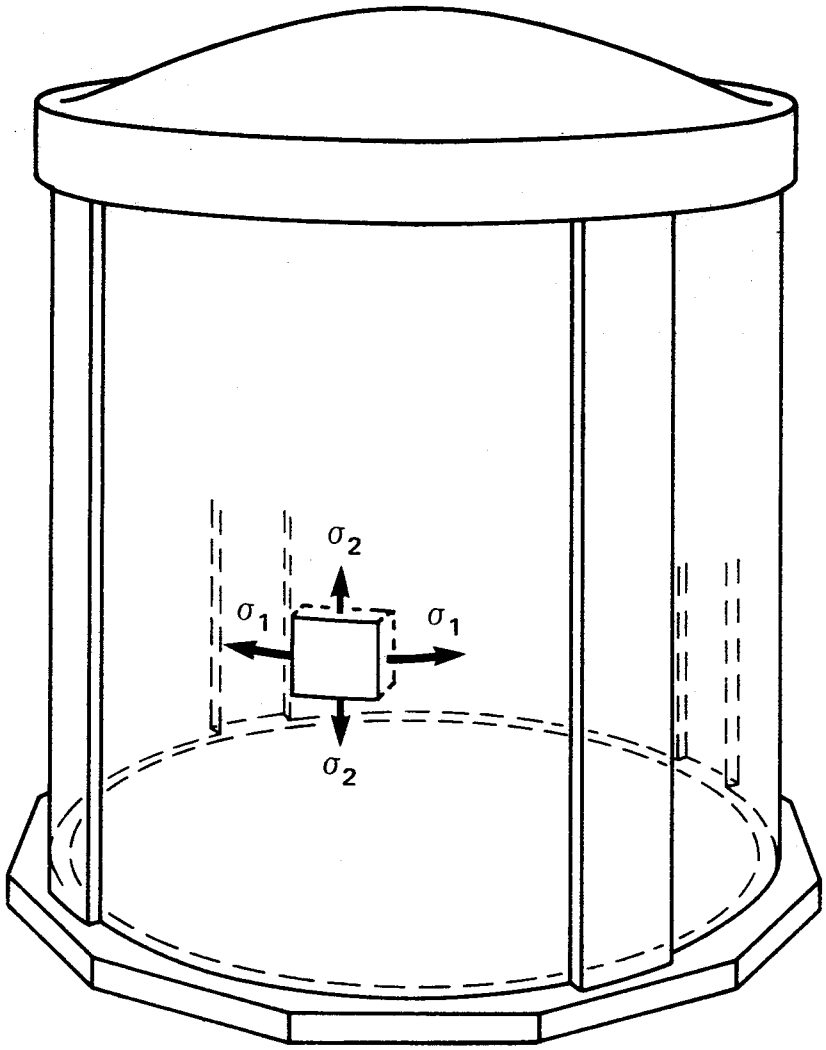

(a) Element in Prototype

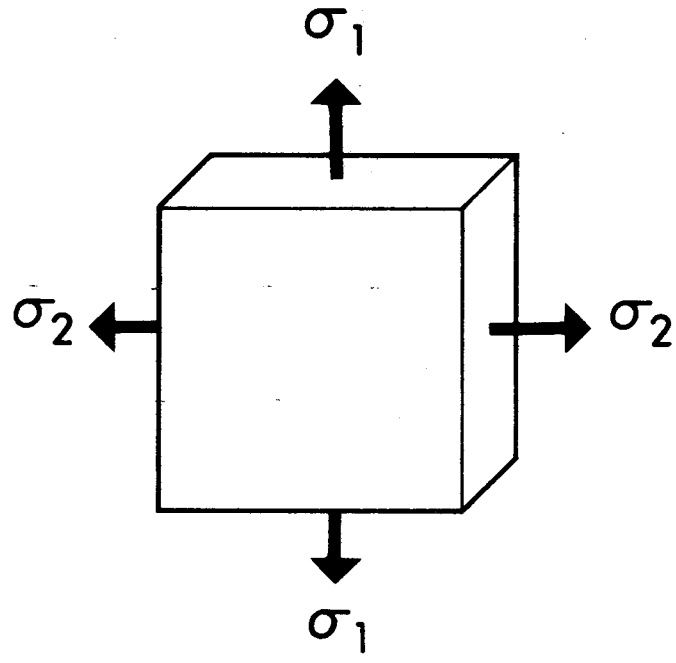

(b) Wall Segment Specimen

Fig. 1.1 Relationship between Specimen and Prototype

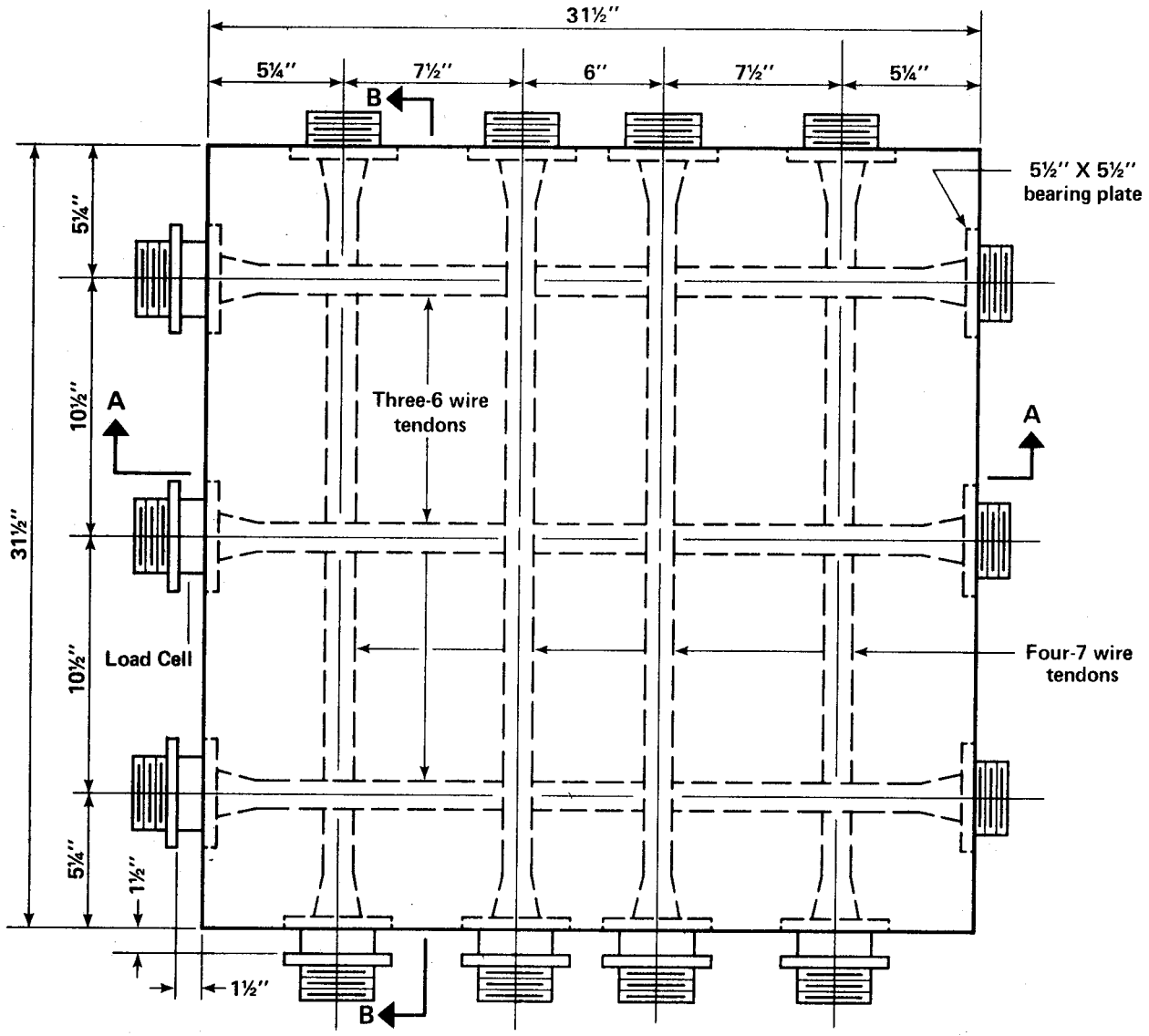

Fig. 2.1 Side View of Wall Segment Specimens

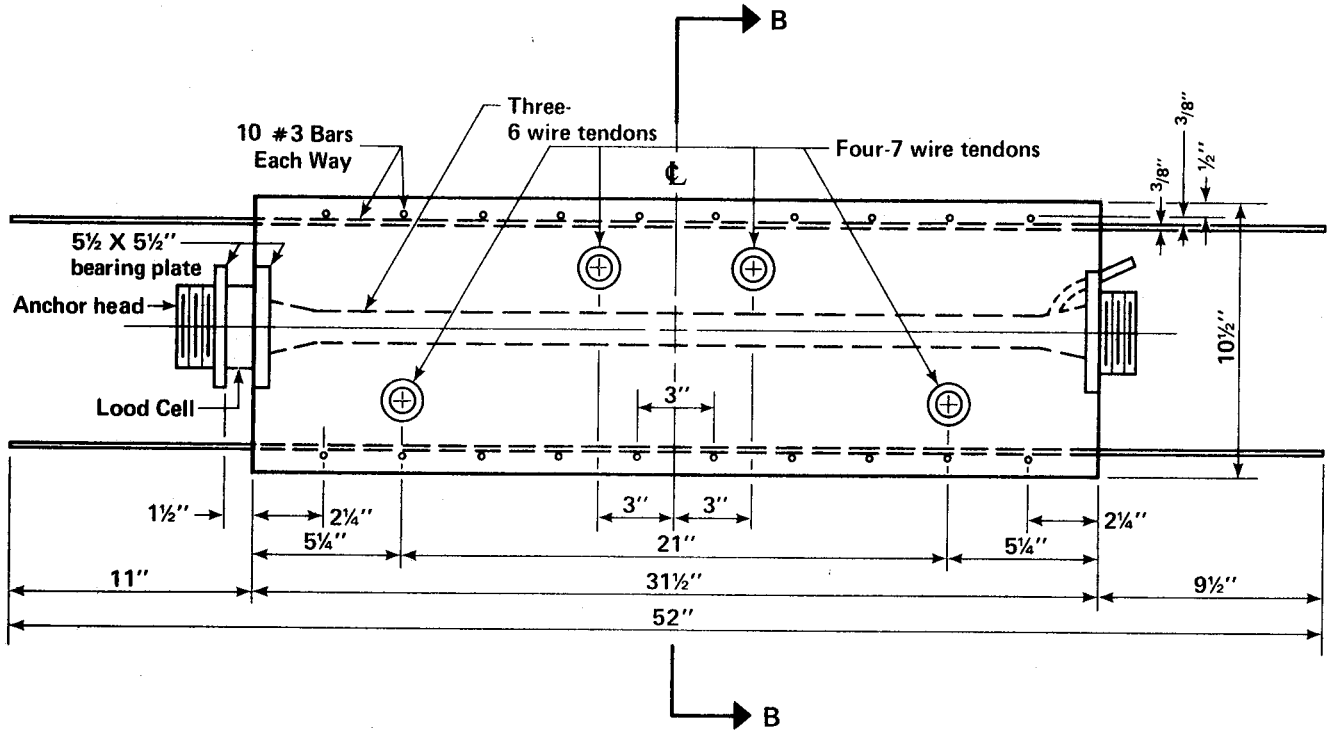

(a) Section A-A

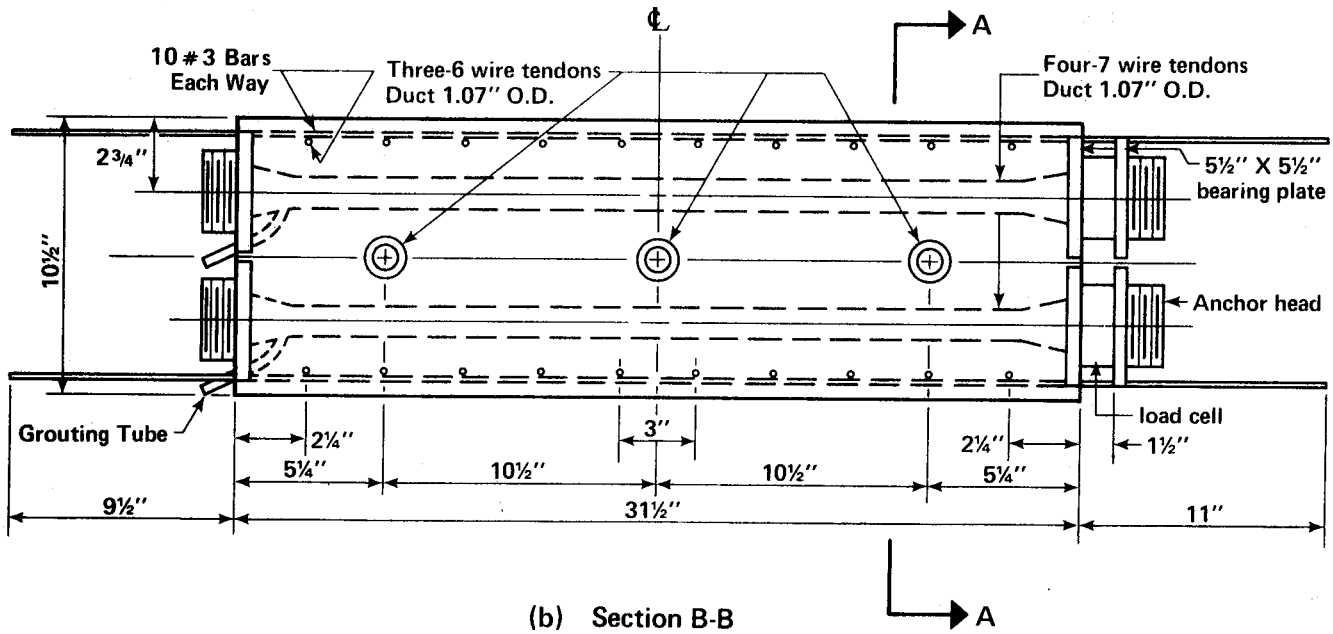

(b) Section B-B

Fig. 2.2 Cross-Sections of Wall Segment Specimens

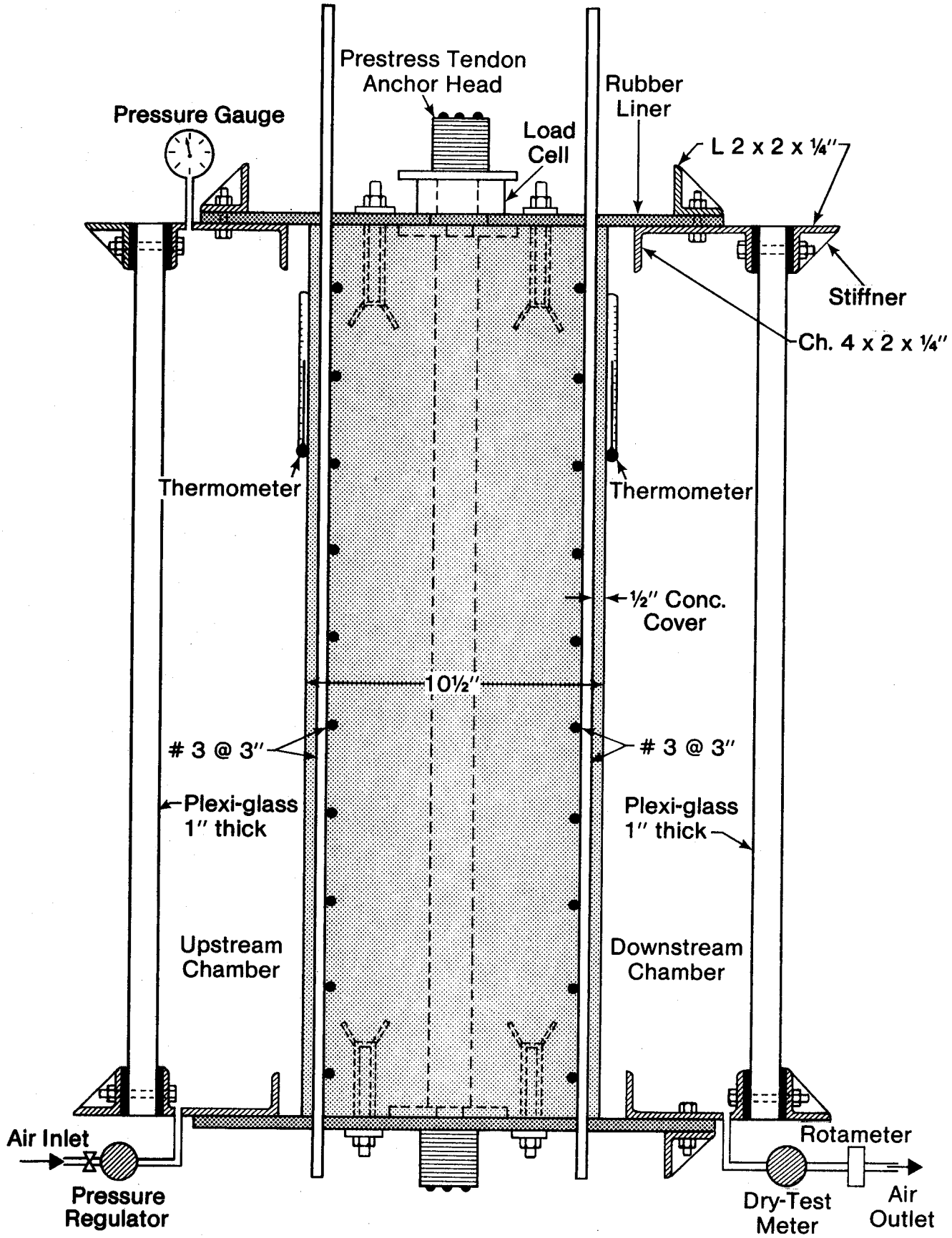

Fig. 2.3 Details of Air Chambers and Rubber Liners, Segment 10

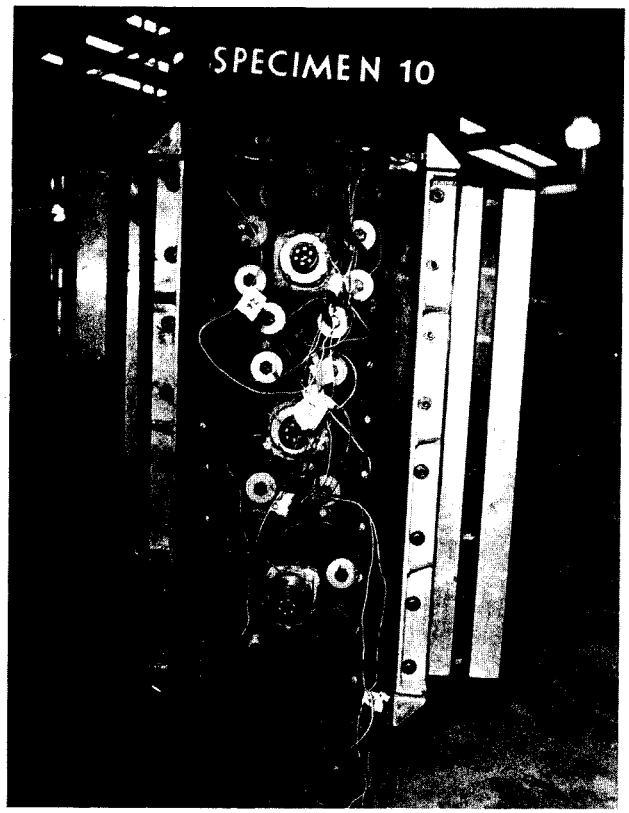

Fig. 2.4 Edge of Segment 10 showing Air Chambers and Rubber Liner

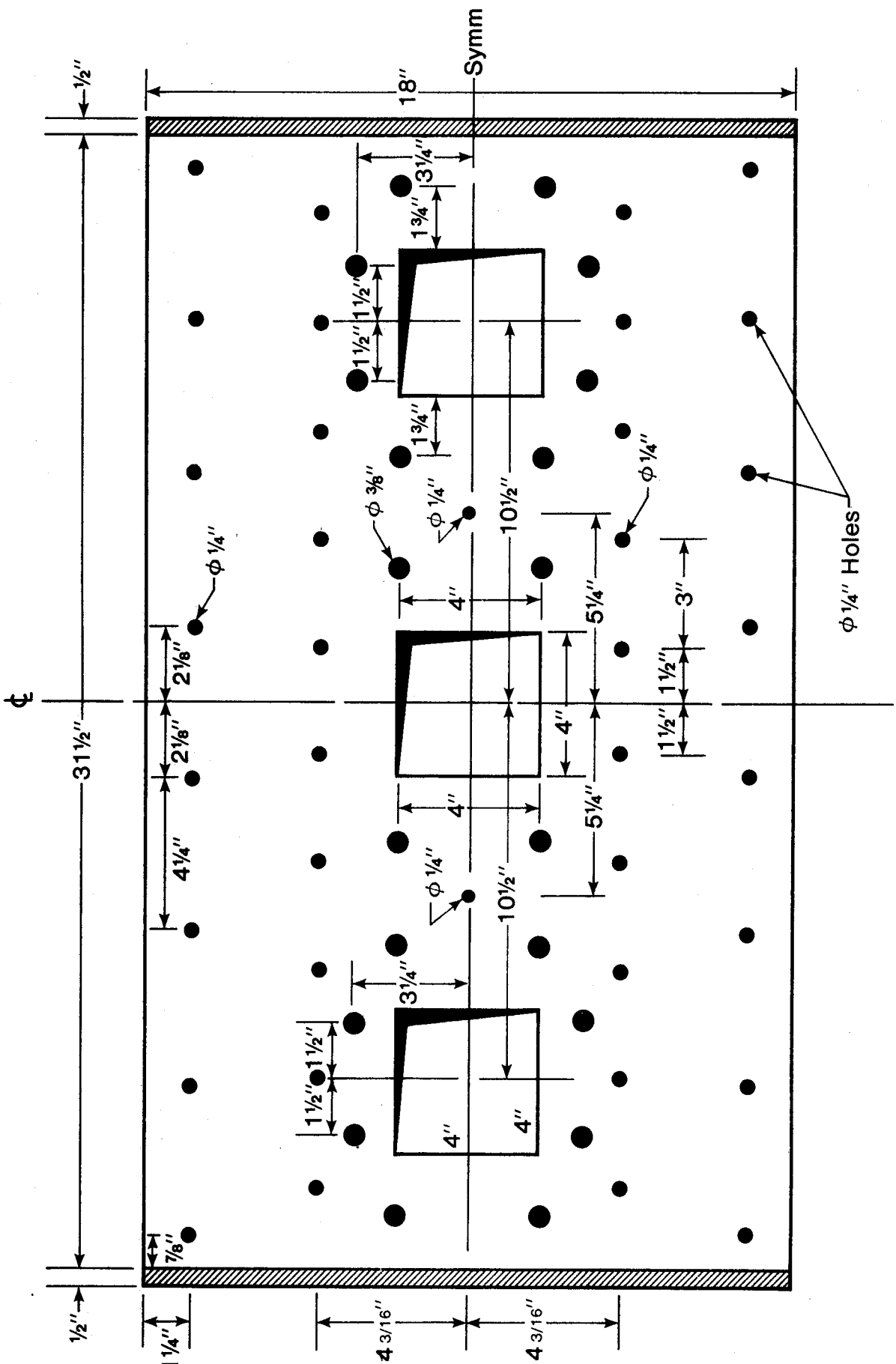

Fig. 2.5 Details of Rubber Liner on Edge with Three Tendons

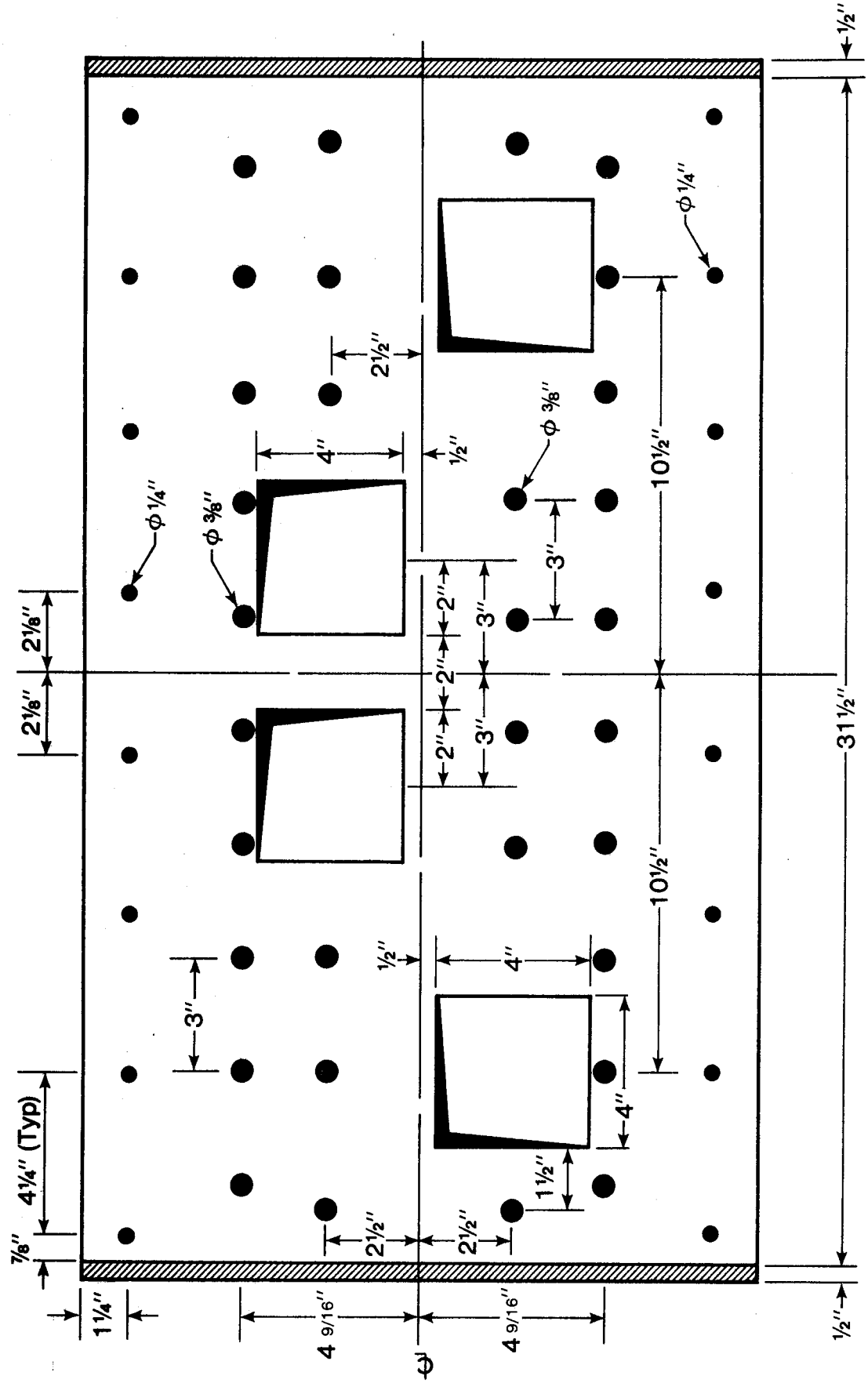

Fig. 2.6 Details of Rubber Liner on Edge with Four Tendons

Figure 2.7 Segment 10 Prior to Casting

Fig. 2.8 Attachment of the Rubber Liner
to the Plywood Form

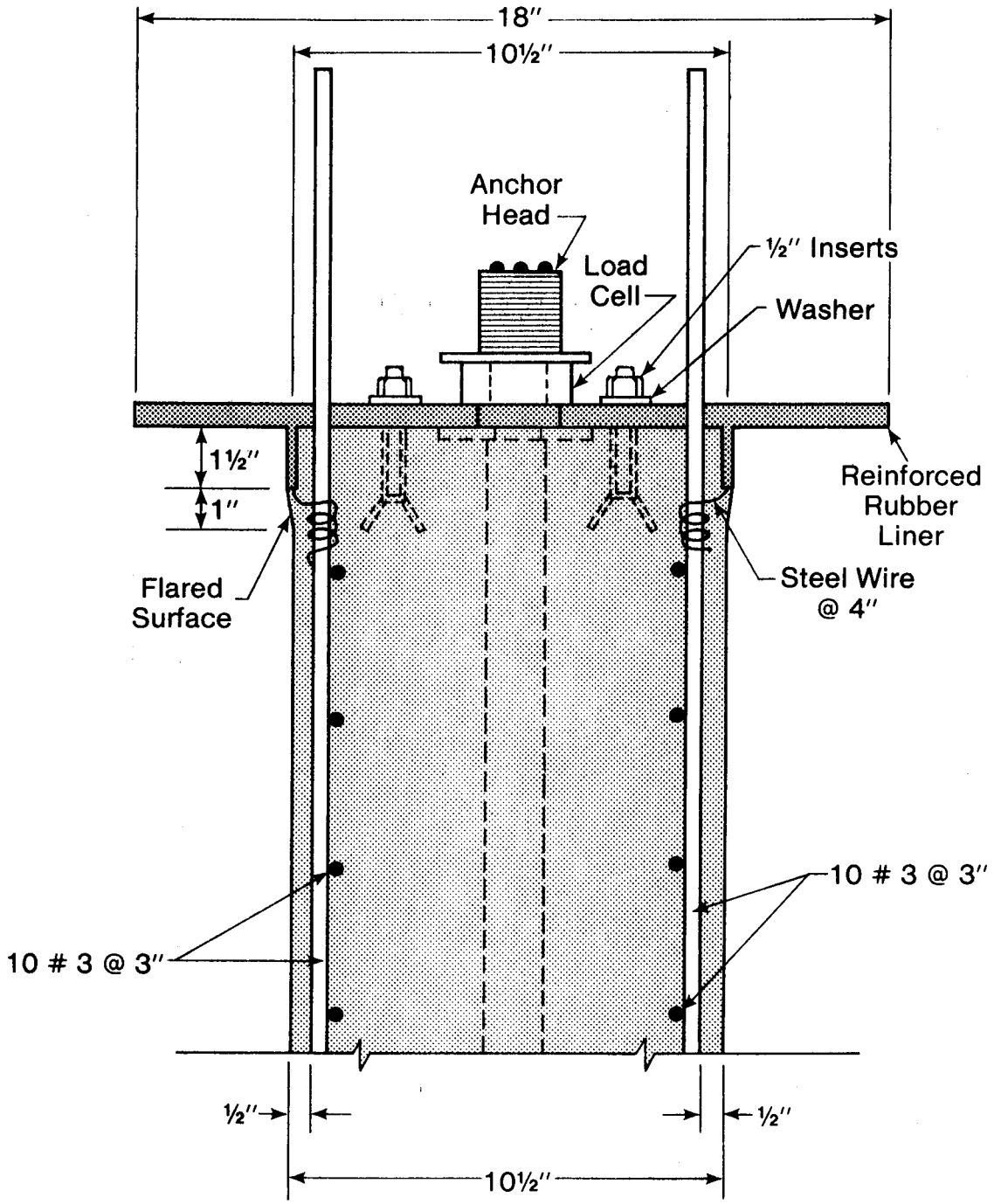

Fig. 2.9 Details of Rubber Liner, Segment 14

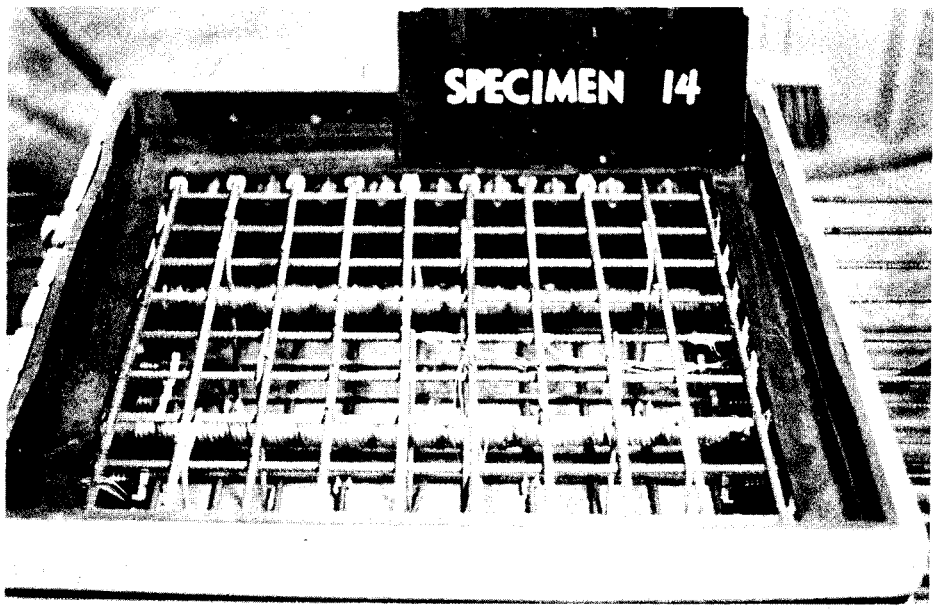

Figure 2.10 Segment 14 Prior to Casting Concrete

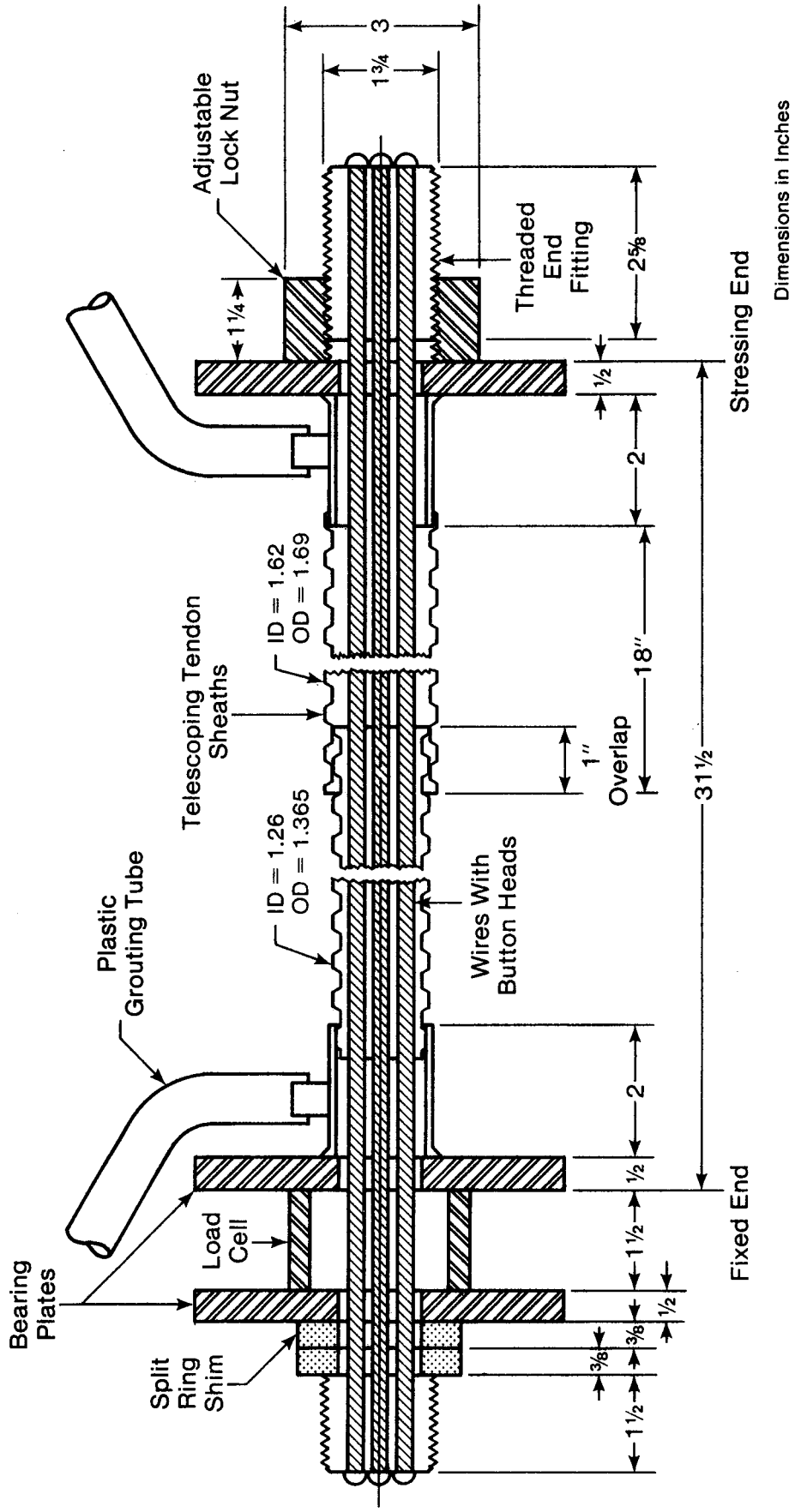

Figure 2.11 Prestressing Tendon Assembly

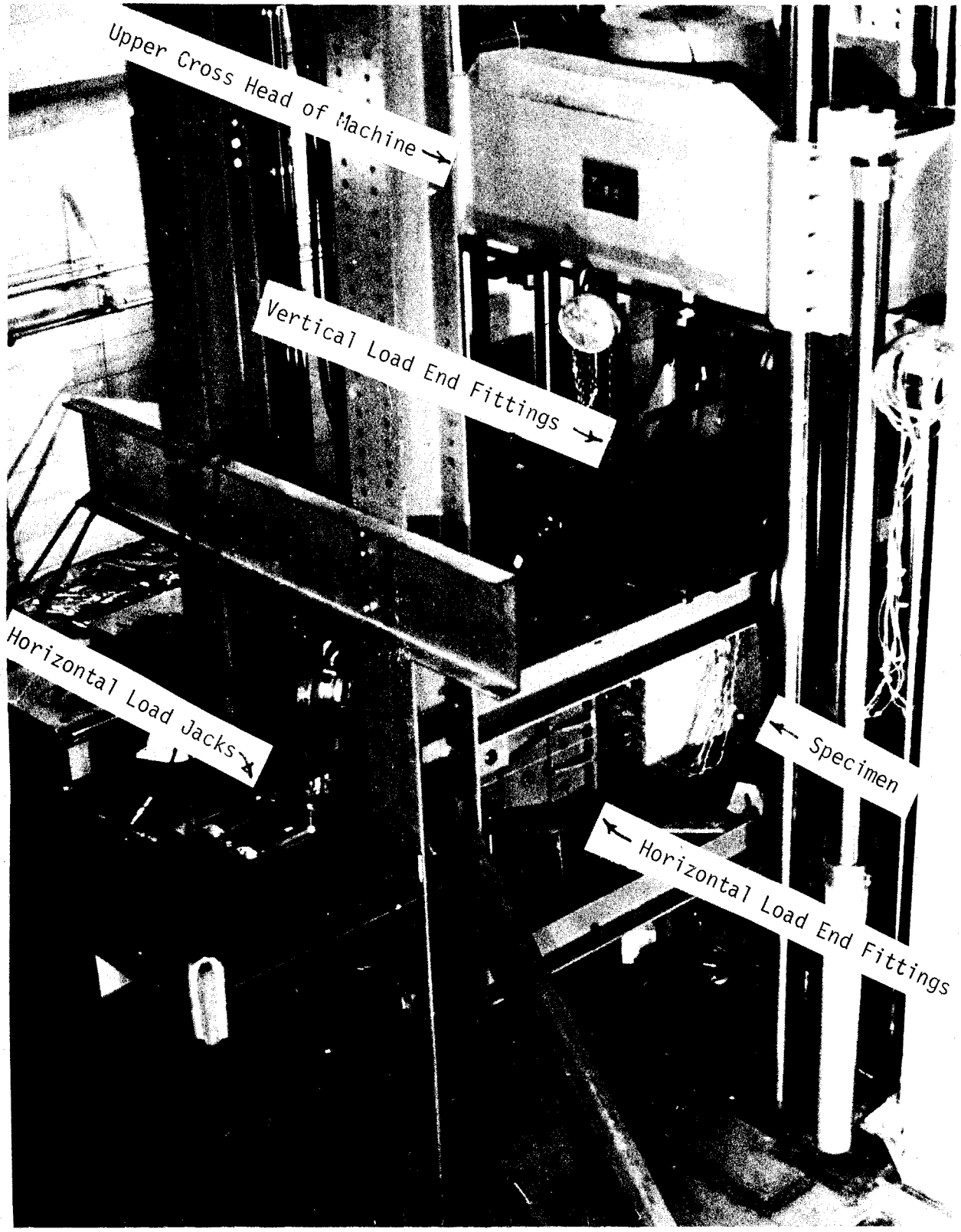

Fig. 3.1 Test Apparatus

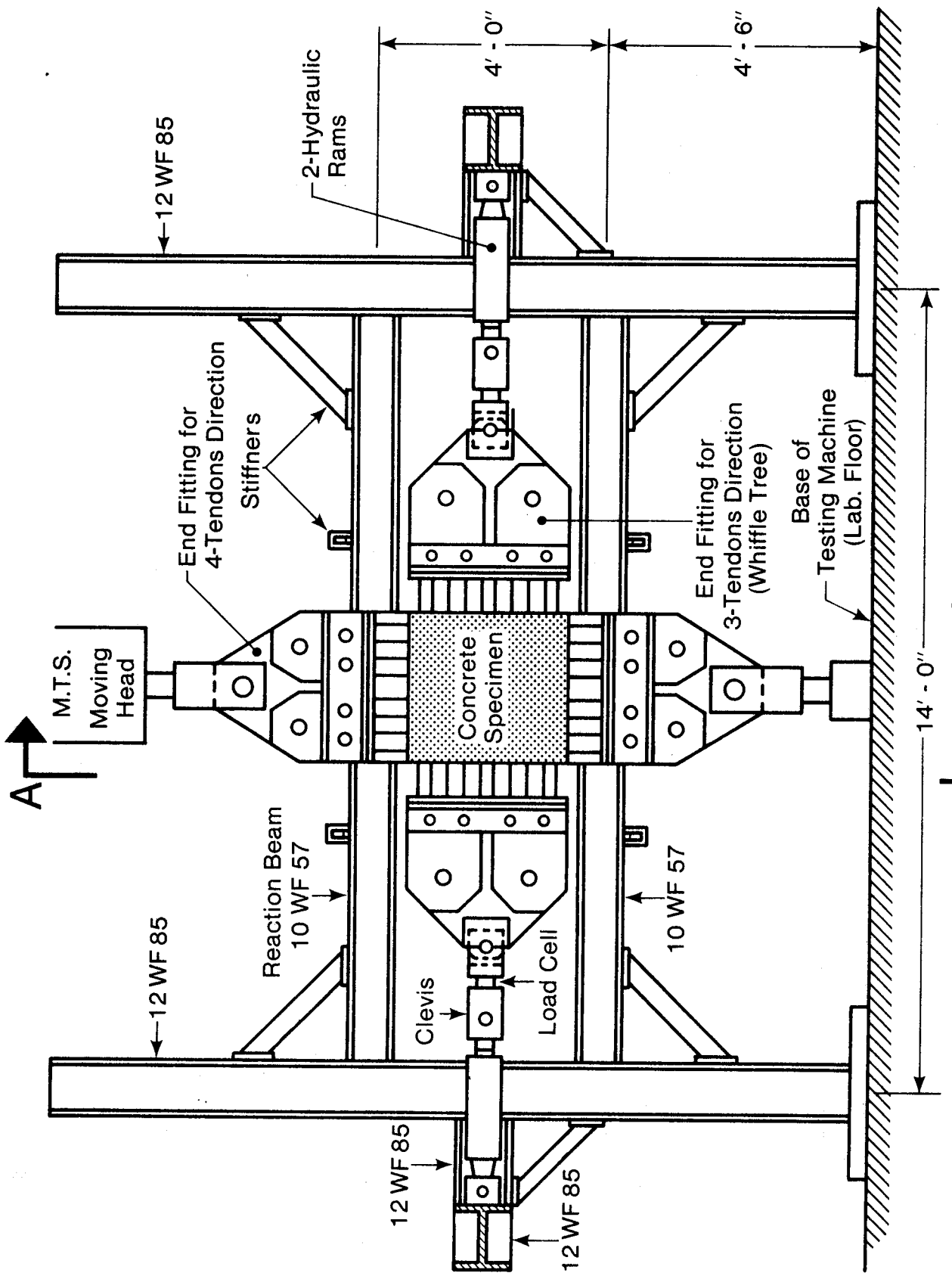

Fig. 3.2 East-West Section Through Loading Frame

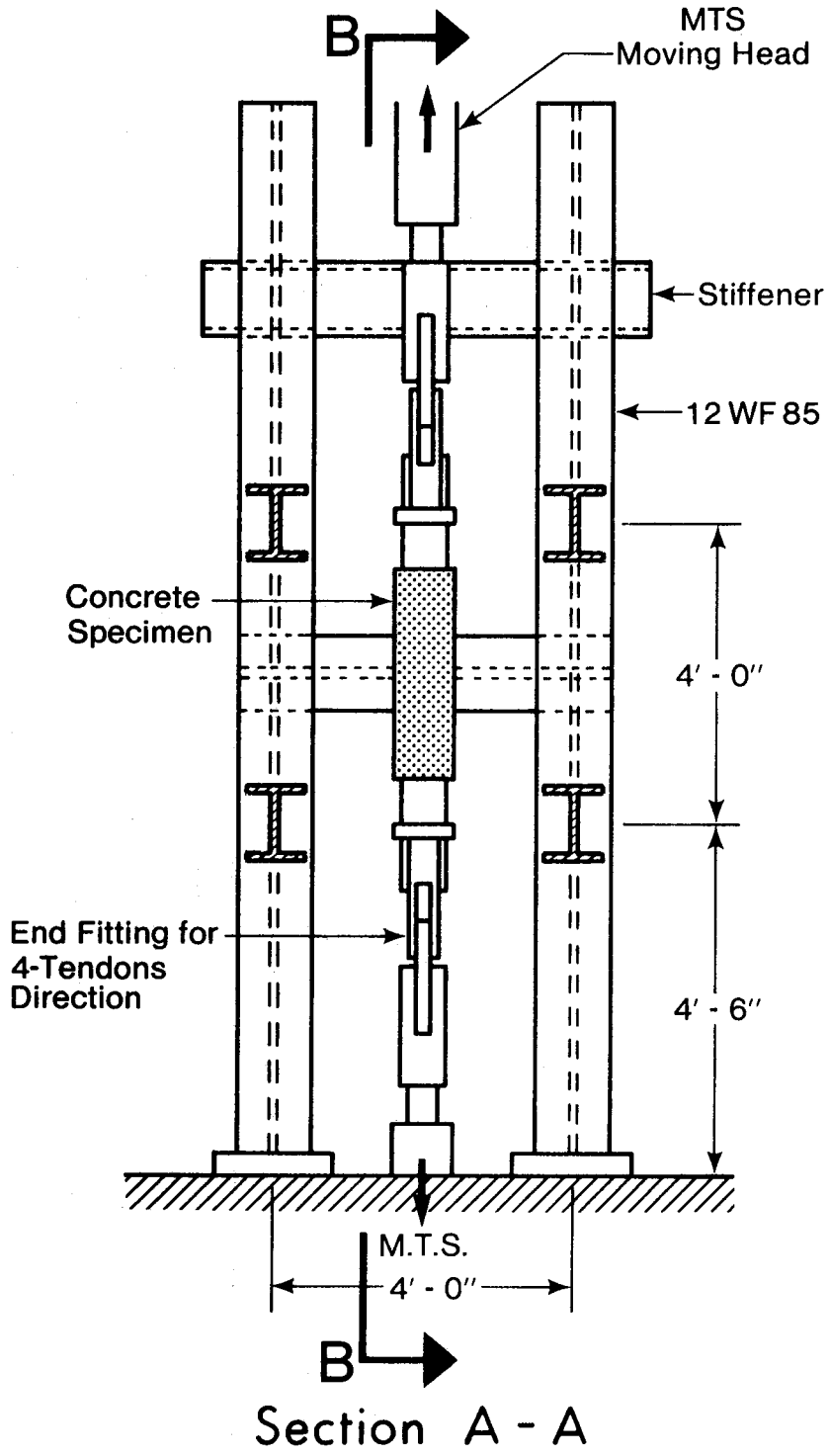

Fig. 3.3 North-South Section Through Loading Frame

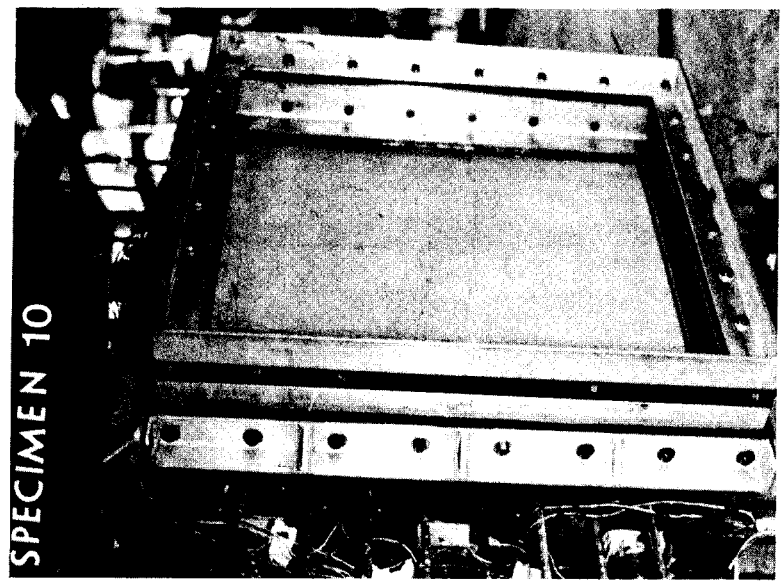

Figure 3.5 Downstream Air Chamber

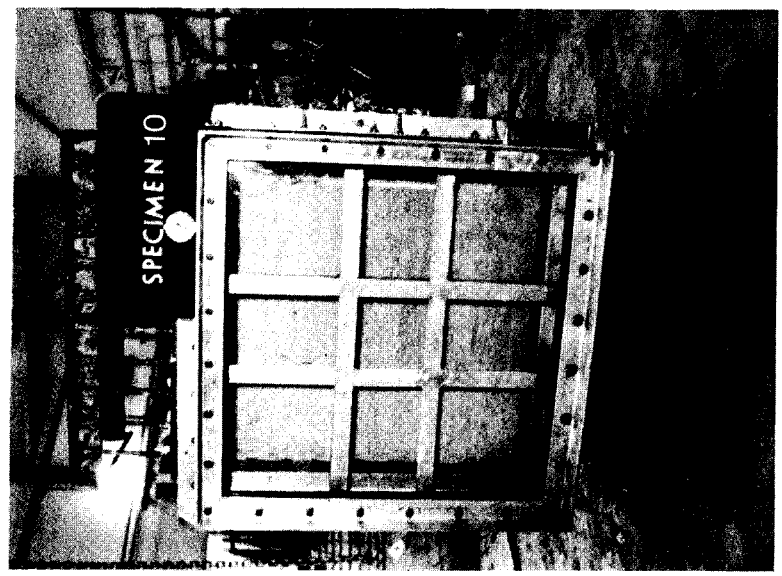

Figure 3.4 Upstream Air Pressure Chamber

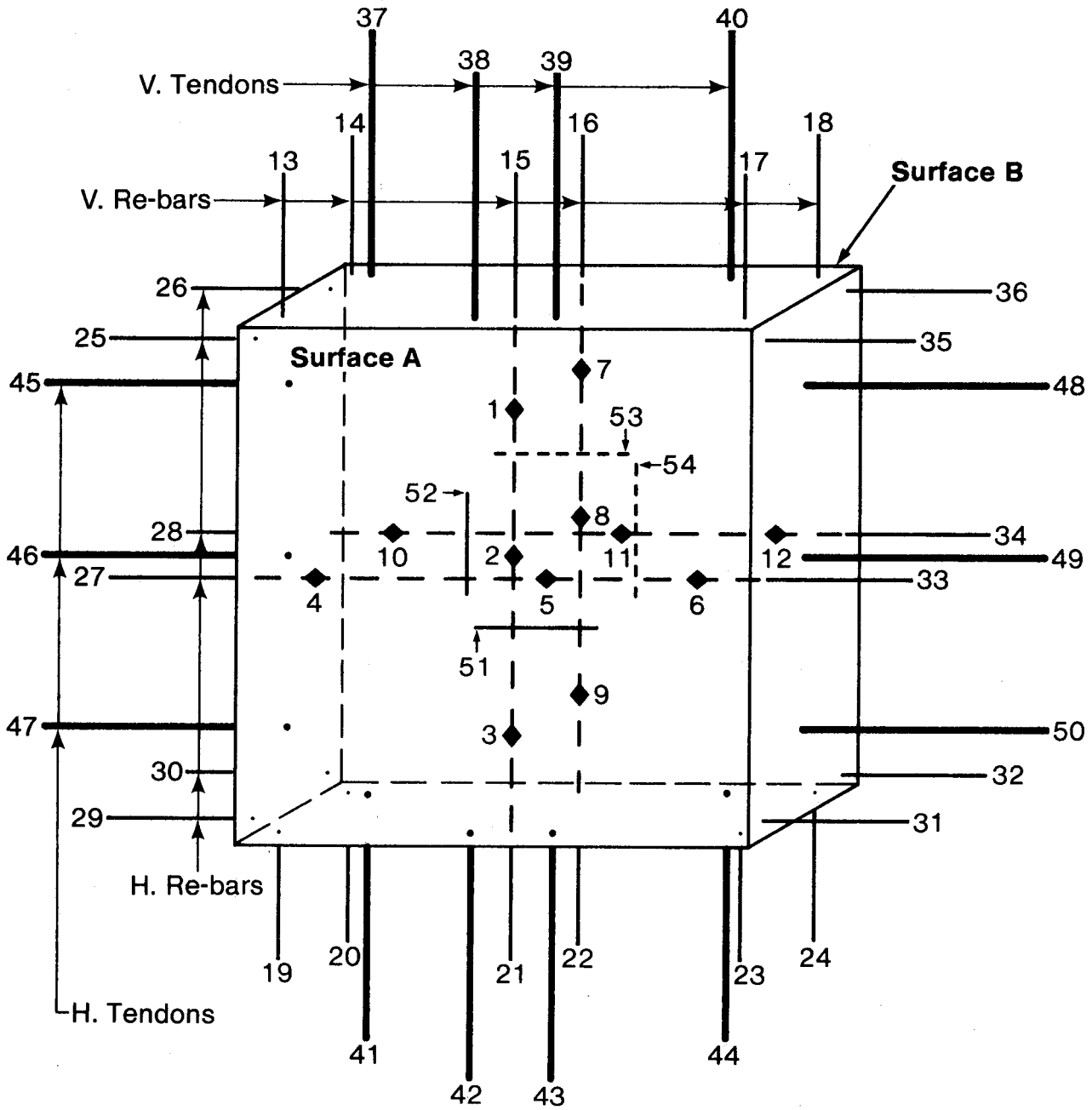

55 West L.C.	59 West Trans.
56 East L.C.	60 East Trans.
57 Top Trans.	61 M.T.S. LD
58 Bot. Trans.	62 M.T.S. ST

◆◆ Embeded Steel Electric Strain Gauges

Concrete Electric Strain Gauges

Fig. 3.6 Location of Electrical Strain Gauges and Transducers, Segment 10

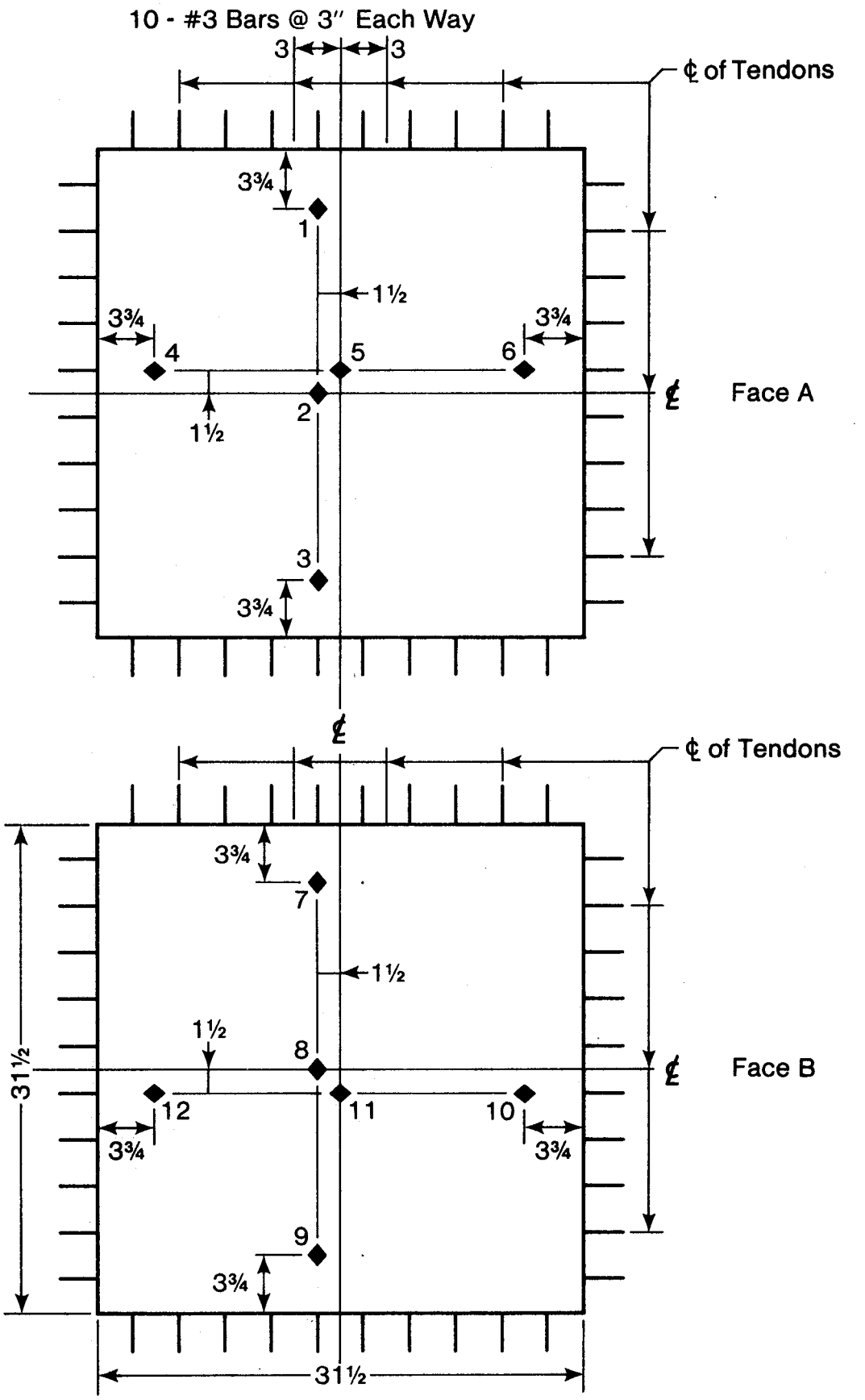

Figure 3.7 Location of Strain Gauges in Segment 10

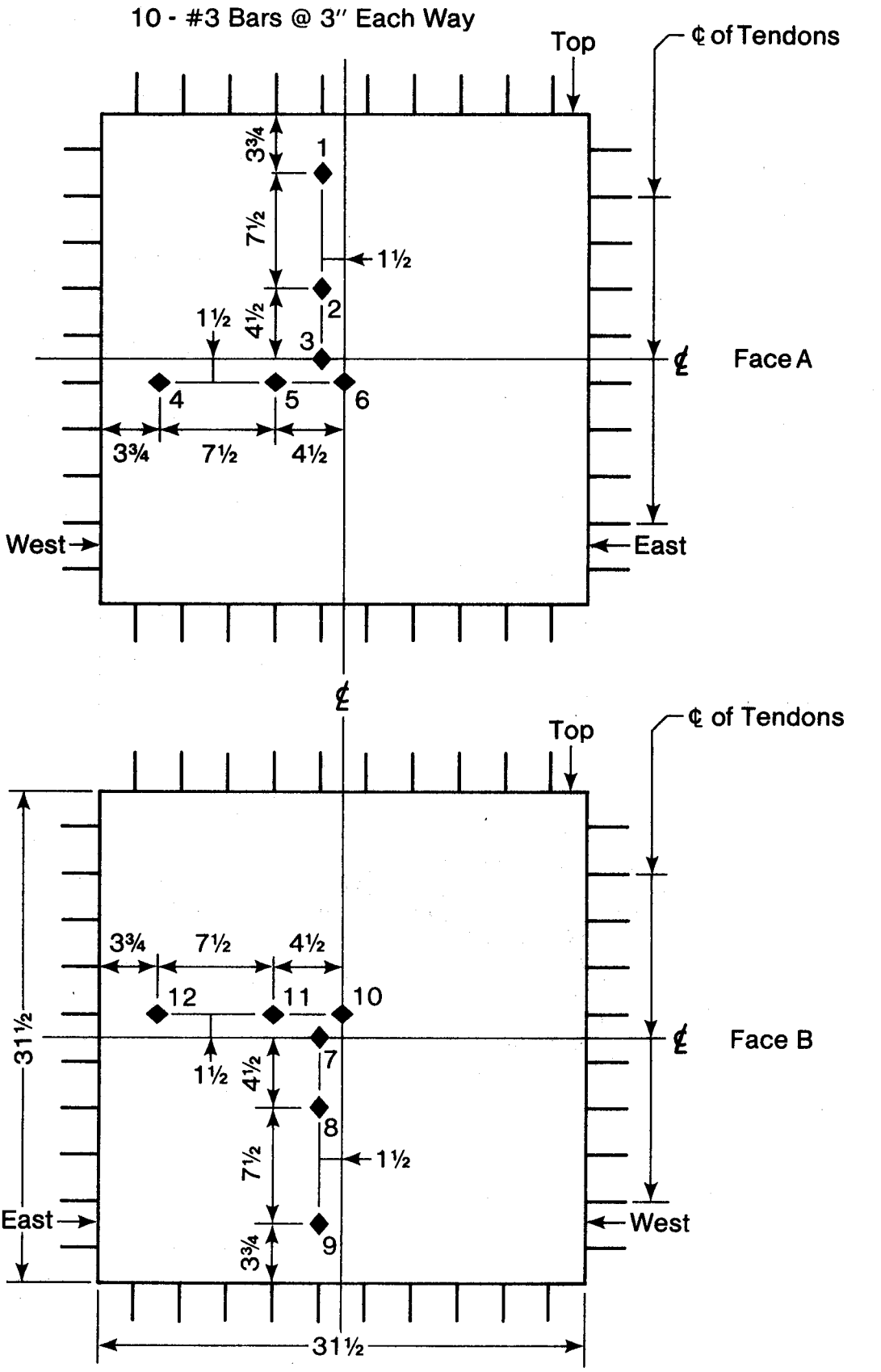

Figure 3.8 Location of Strain Gauges in Segment 14

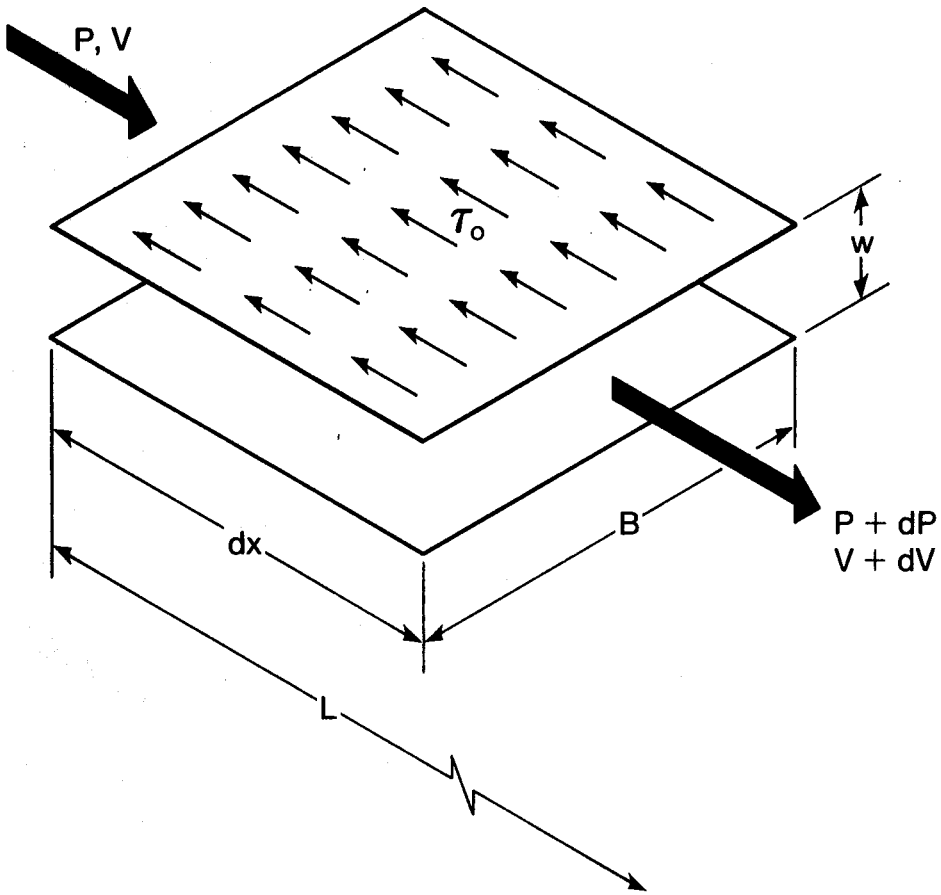

Fig. 4.1 Idealization of Crack as a Gap Between Parallel Plates

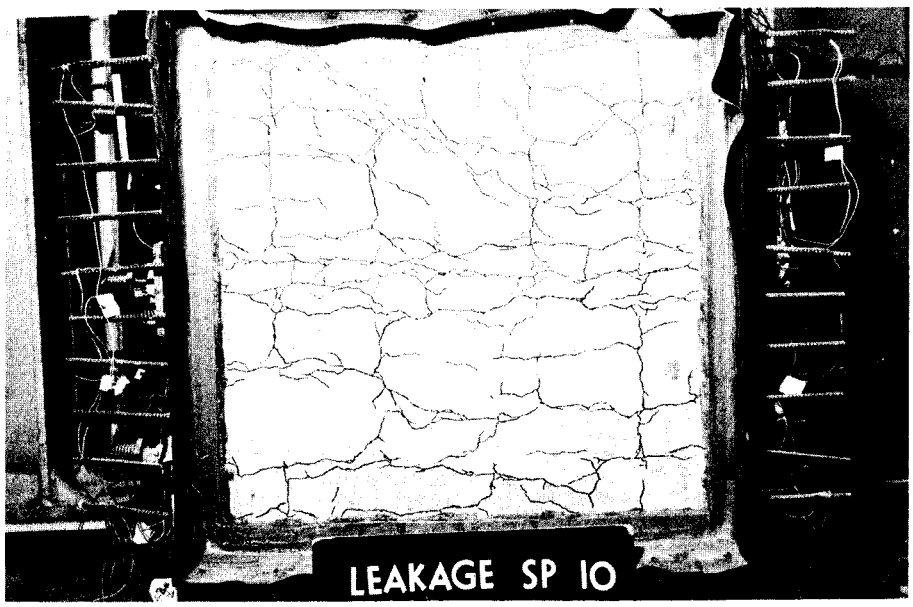

Fig. 5.1 Up-stream Face of Segment 10 after Testing

Fig. 5.2 Down-stream Face of Segment 10 after Testing

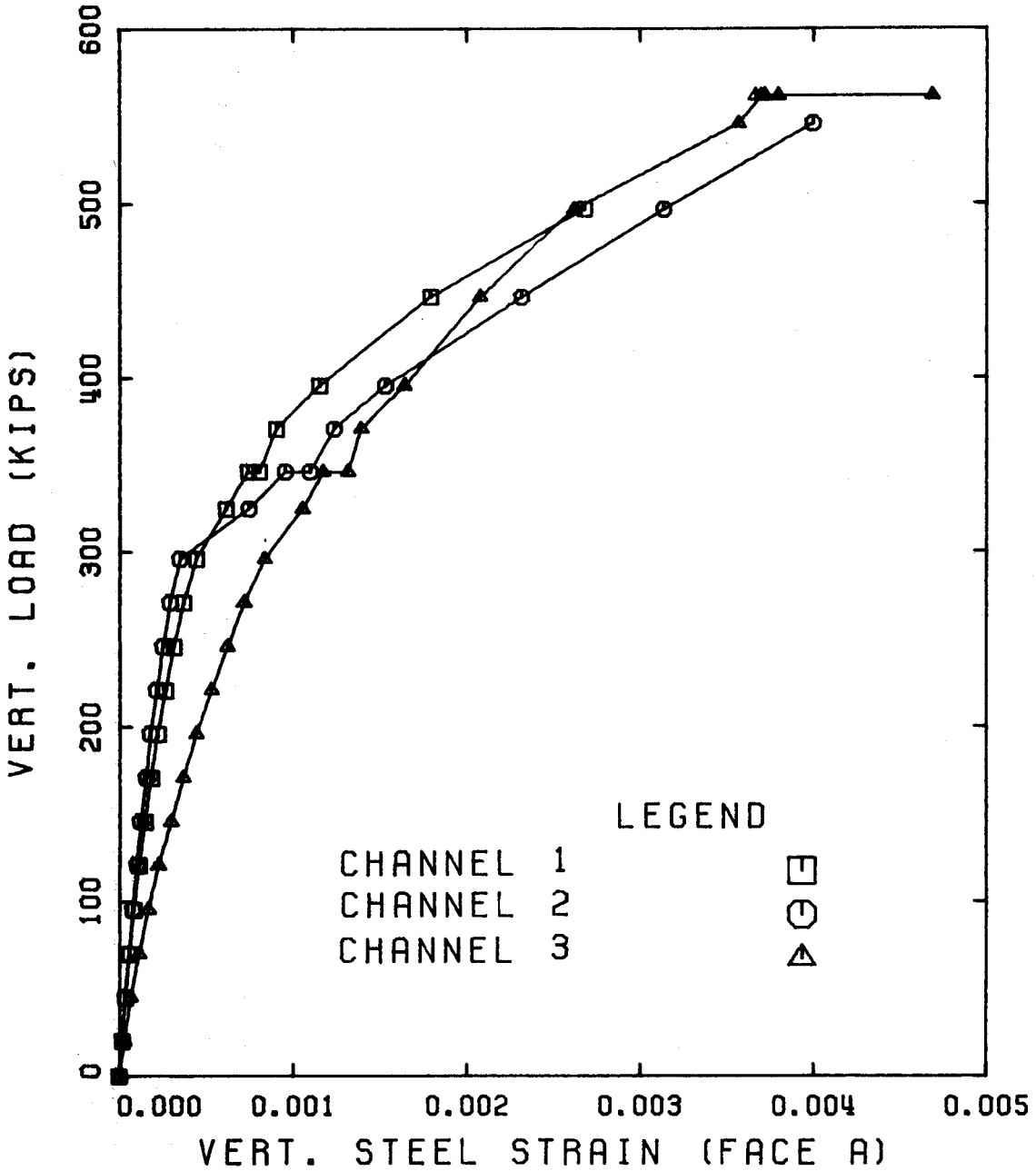

Fig. 5.3 Load-Strain Curves for Individual Embedded Strain Gauges in Vertical Direction, Specimen 10, Face A

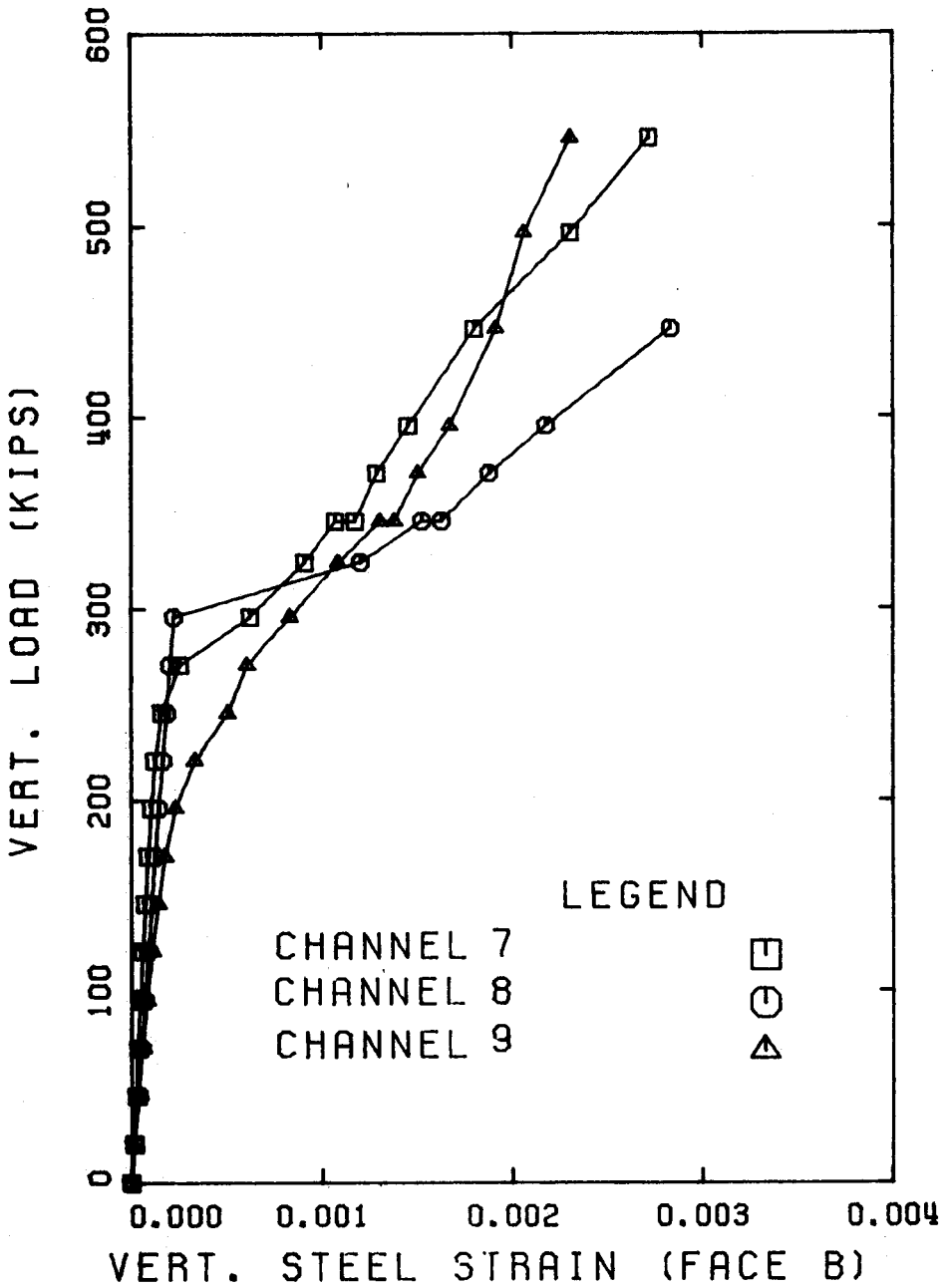

Fig. 5.4 Load-Strain Curves for Individual Embedded Strain Gauges in Vertical Direction, Segment 10, Face B

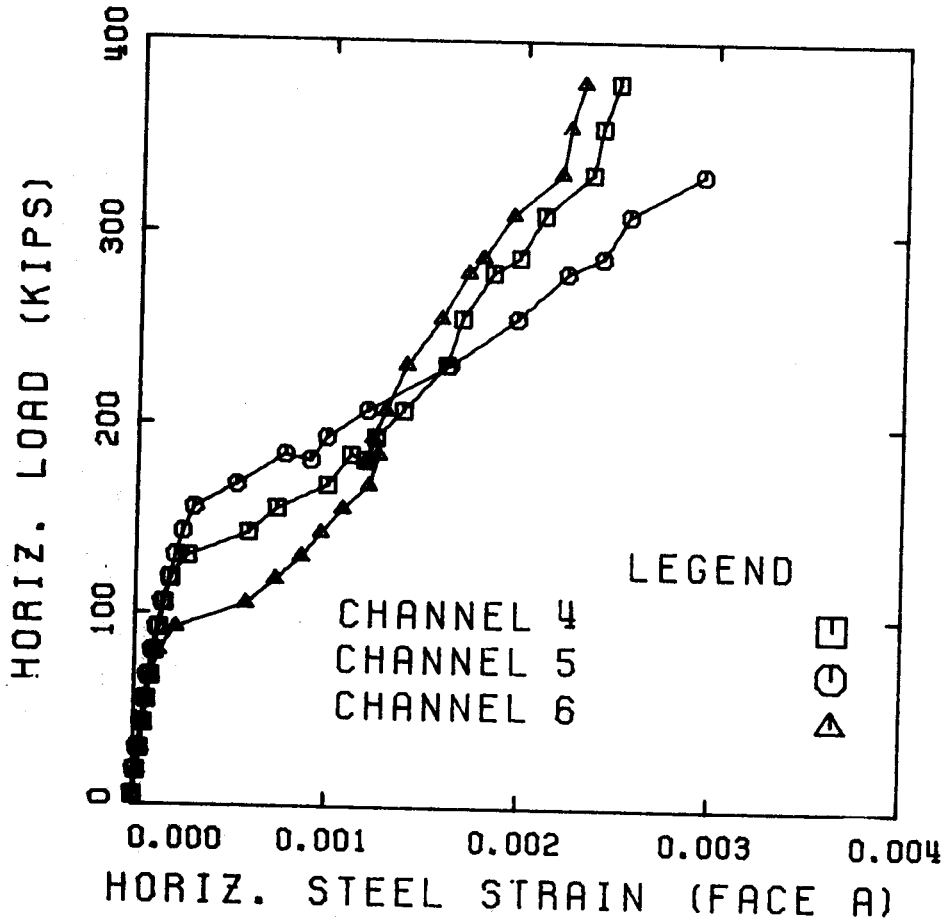

Fig. 5.5 Load-Strain Curves for Individual Embedded Strain Gauges in Horizontal Direction, Segment 10, Face A

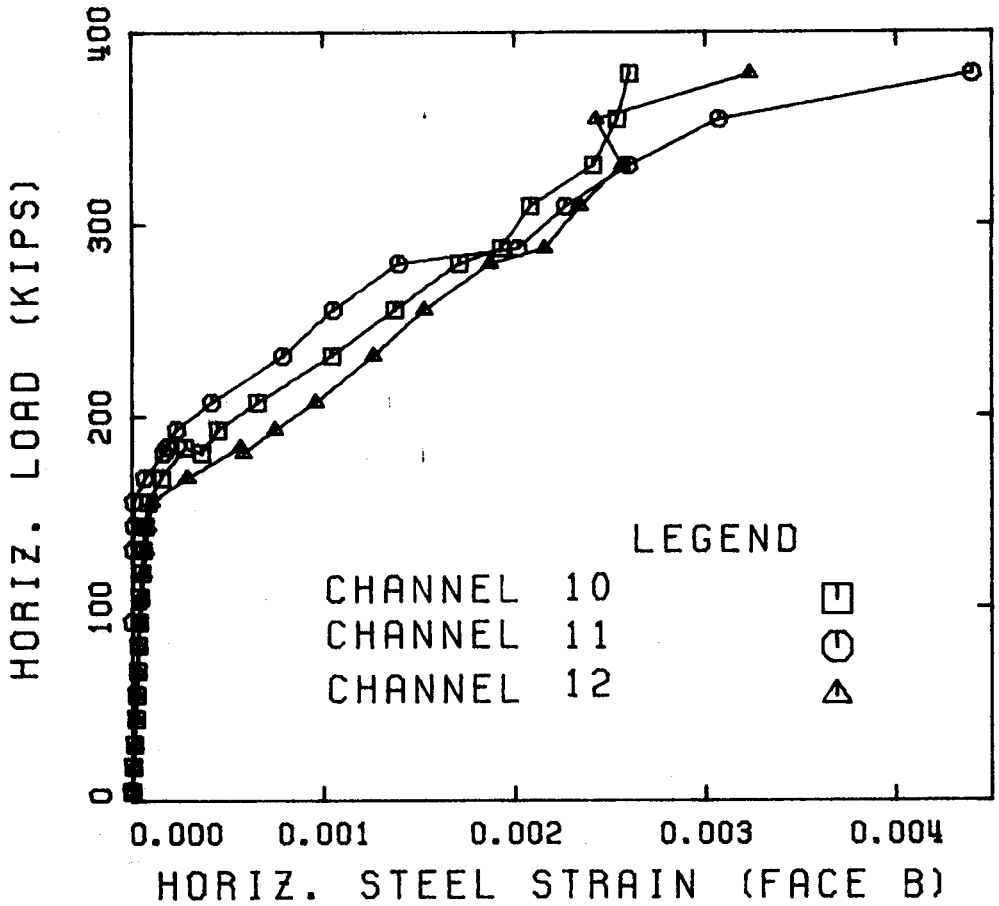

Fig. 5.6 Load-Strain Curves for Individual Embedded Strain Gauges in Horizontal Direction, Segment 10, Face B

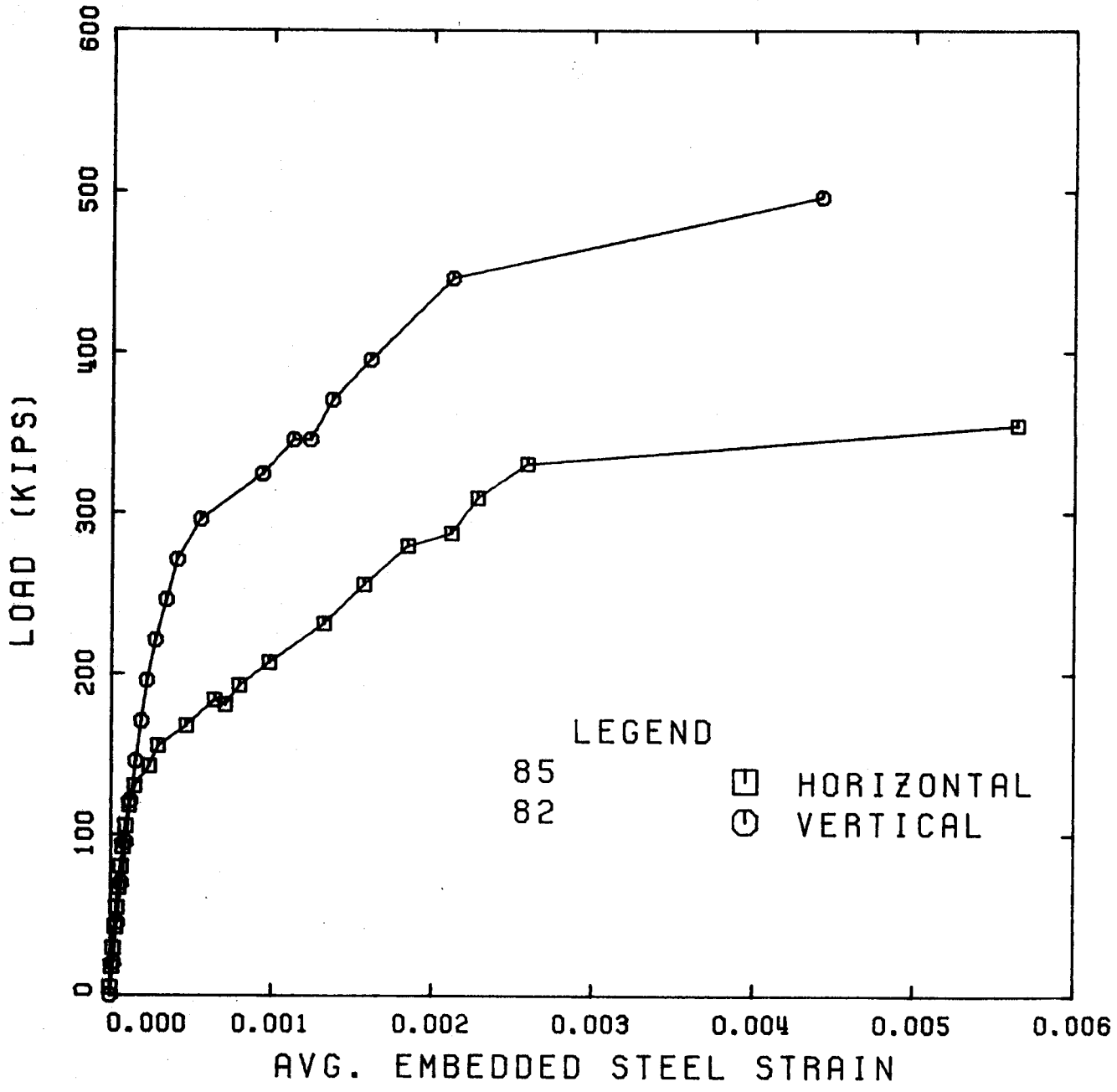

Fig. 5.7 Load-Average Strain Curves, Segment 10

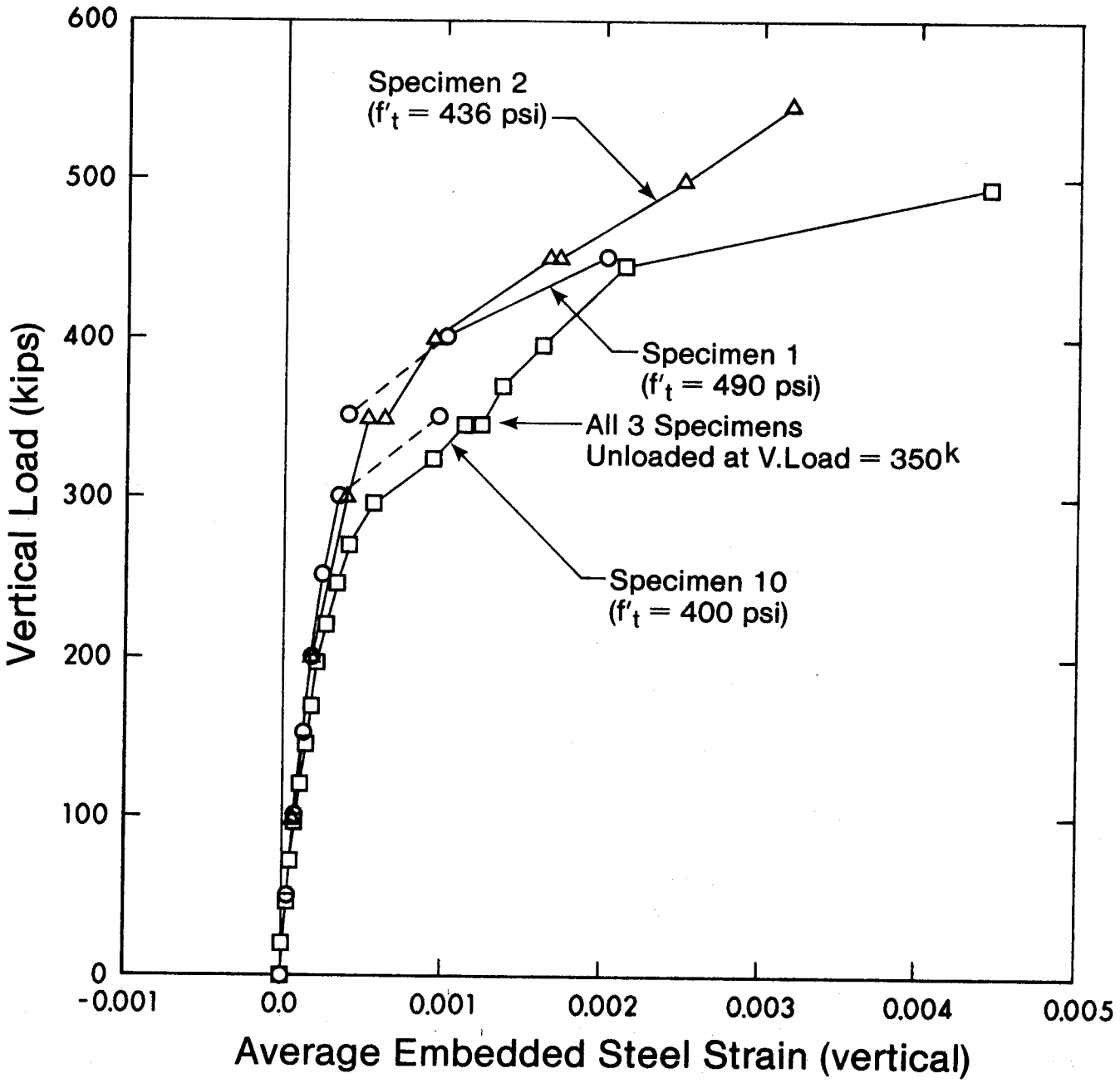

Fig. 5.8 Average Vertical Steel Strains for Segments 1, 2, and 10

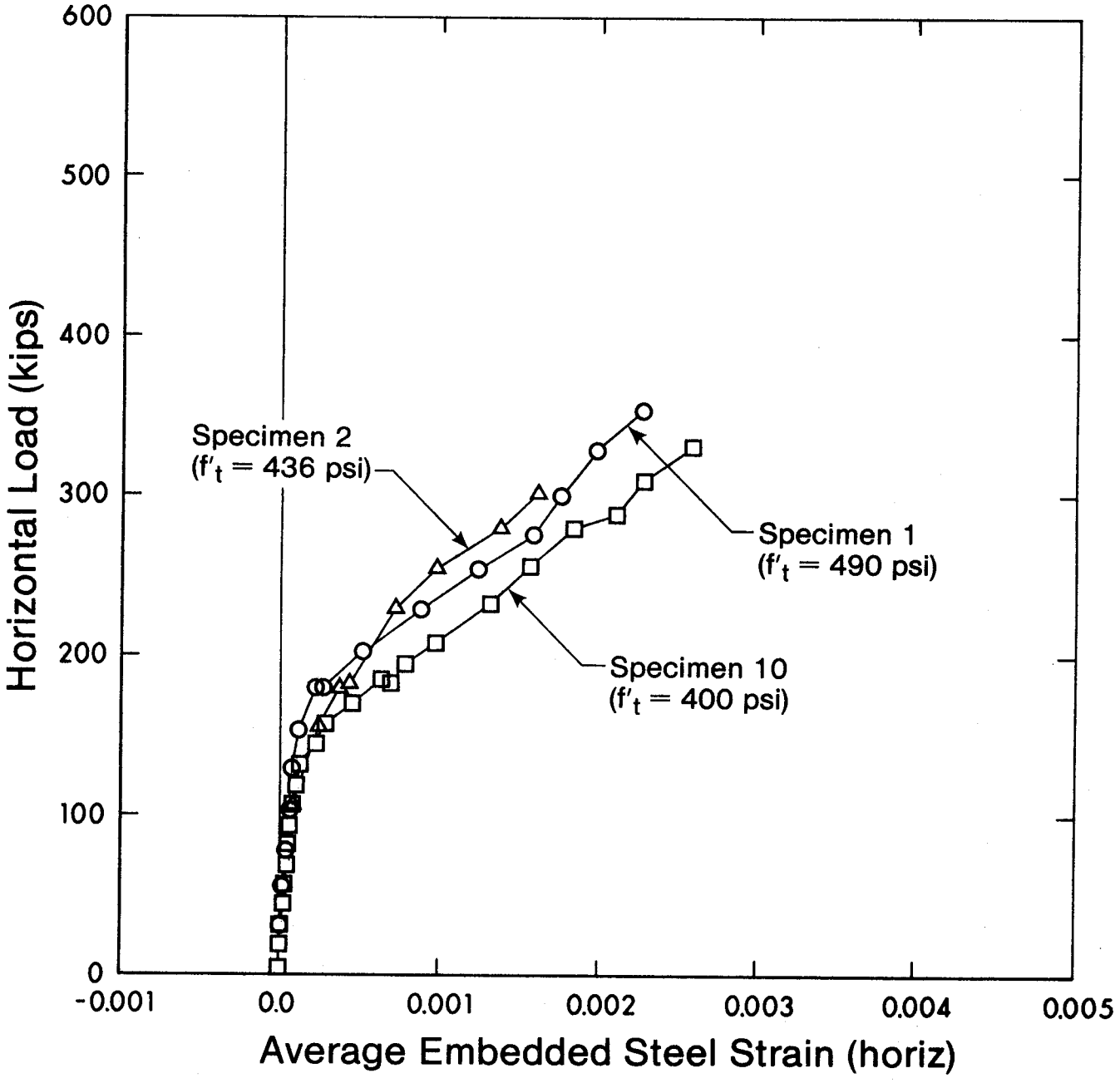

Fig. 5.9 Average Horizontal Steel Strains for Segments 1, 2 and 10

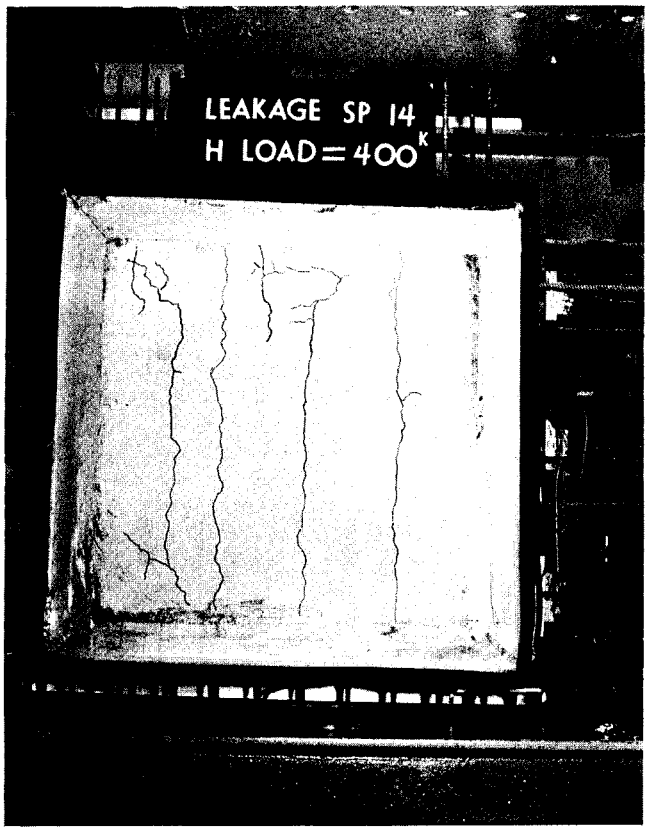

Fig. 5.10 Up-Stream Face of Segment 14 after Testing

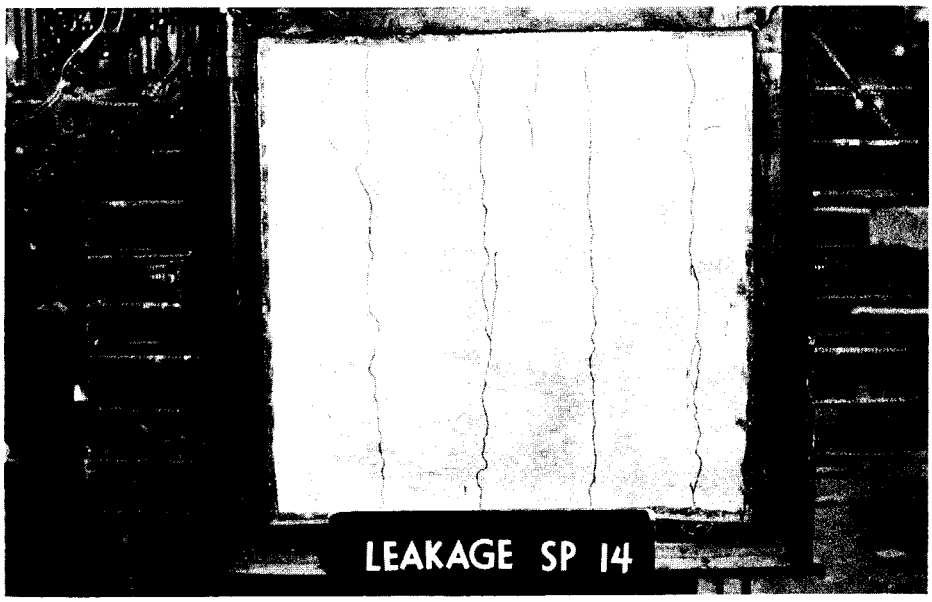

Fig. 5.11 Down-Stream Face of Segment 14 After Testing

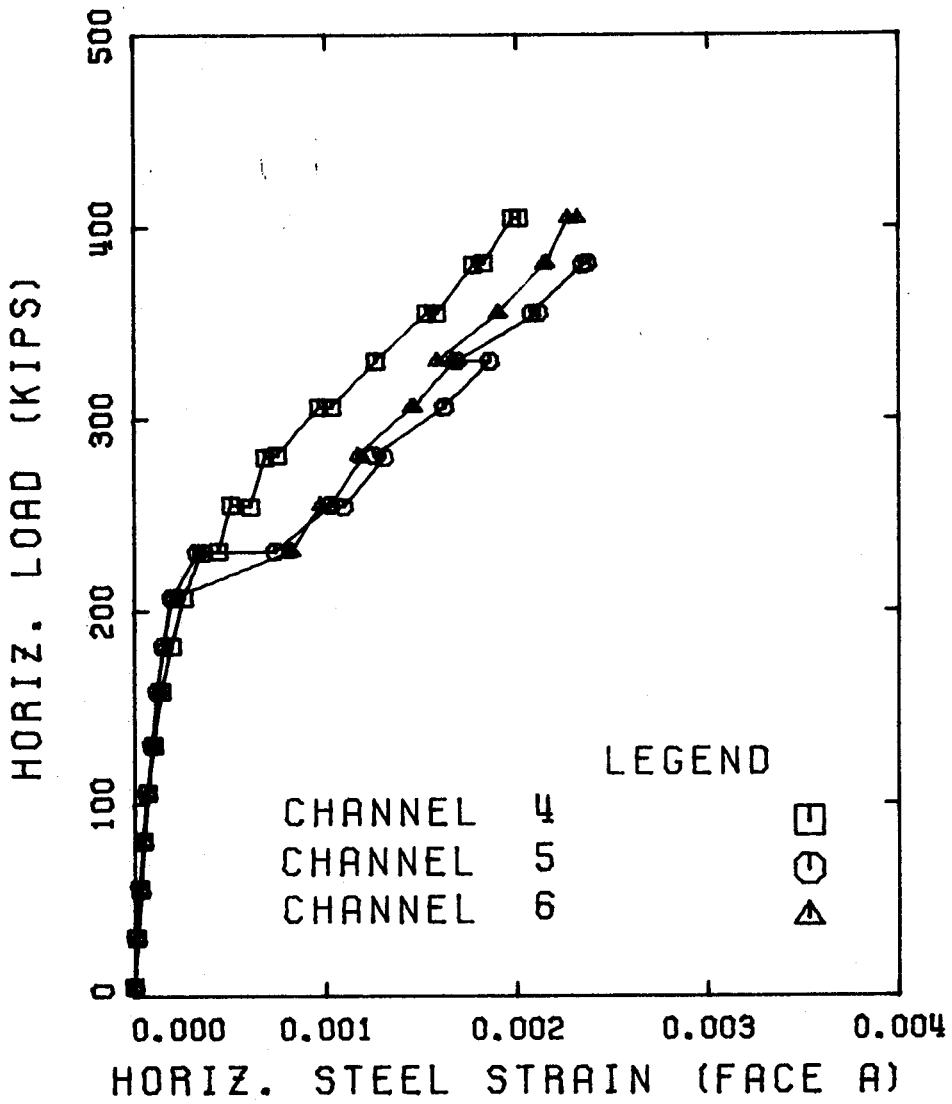

Fig. 5.12 Load-Strain Curves for Individual Embedded Strain Gauges in Horizontal Direction, Segment 14, Face A

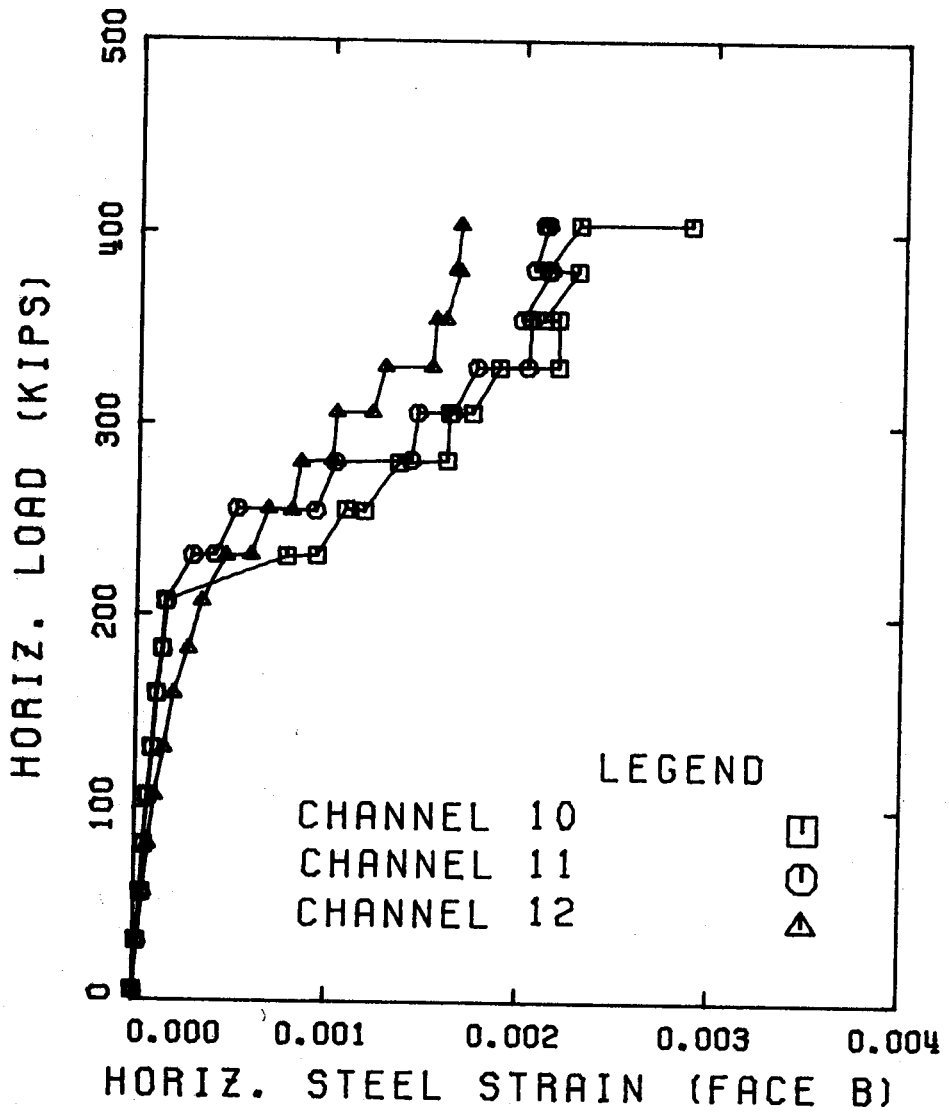

Fig. 5.13 Load-Strain Curves for Individual Embedded Strain Gauges in Horizontal Direction, Segment 14, Face B

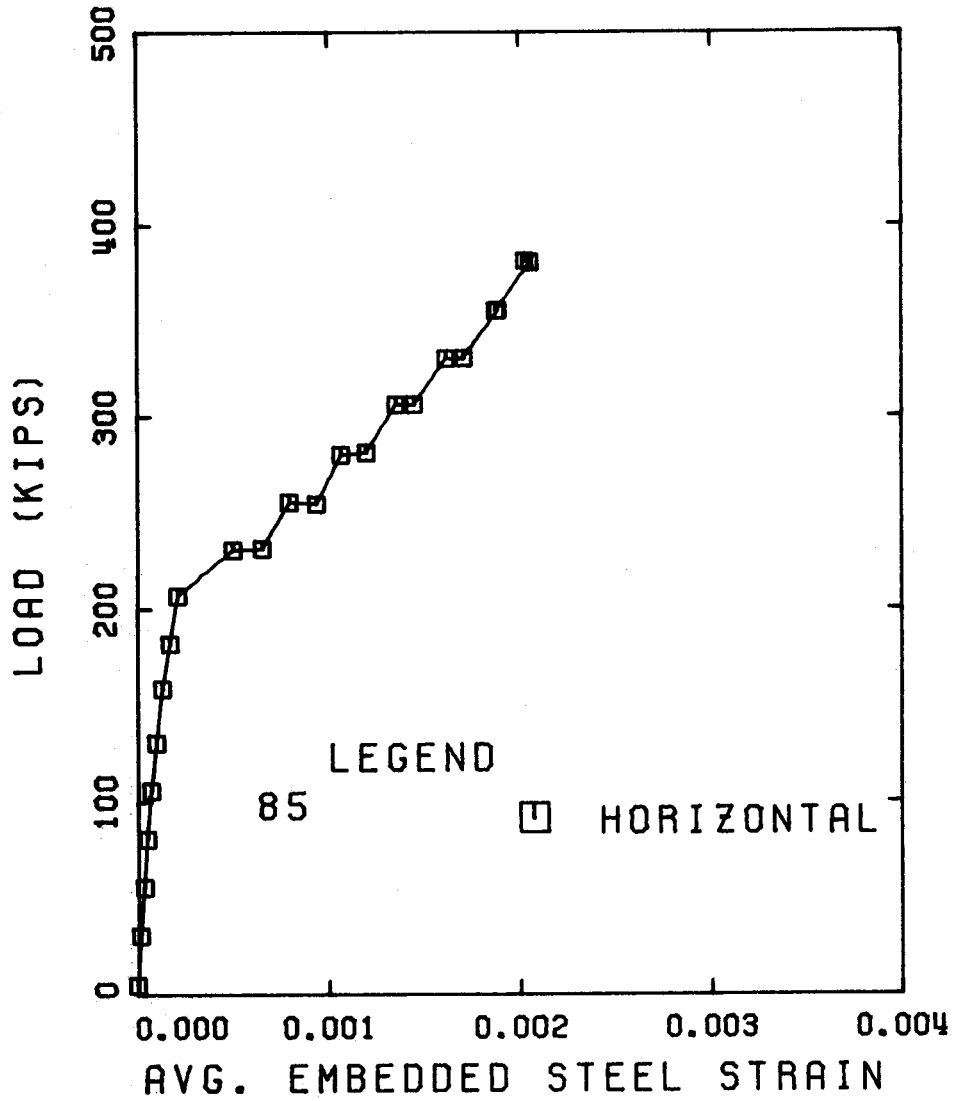

Fig. 5.14 Load-Average Strain Curve, Segment 14

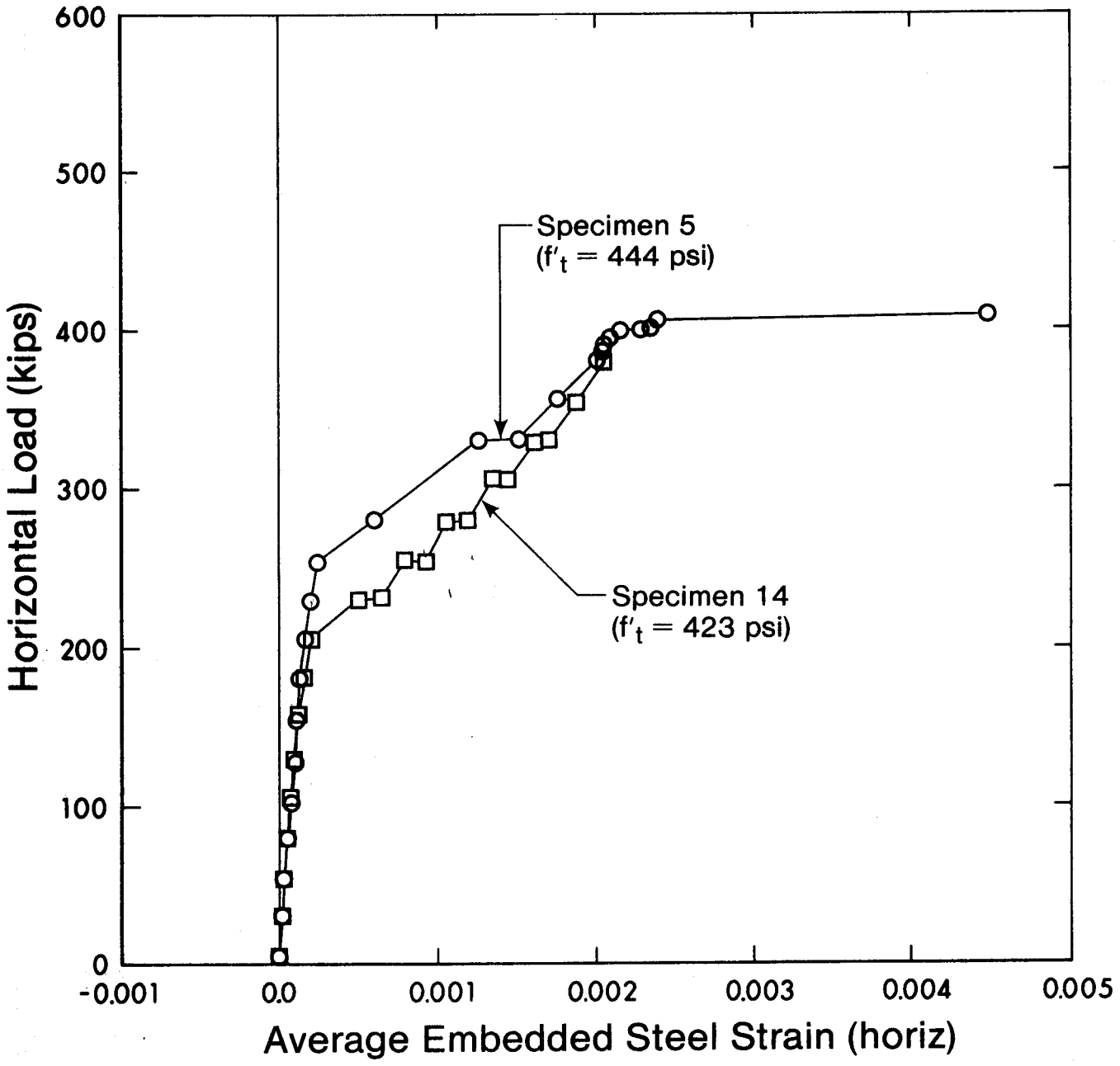

Fig. 5.15 Average Horizontal Steel Strain for Segments 5 and 14

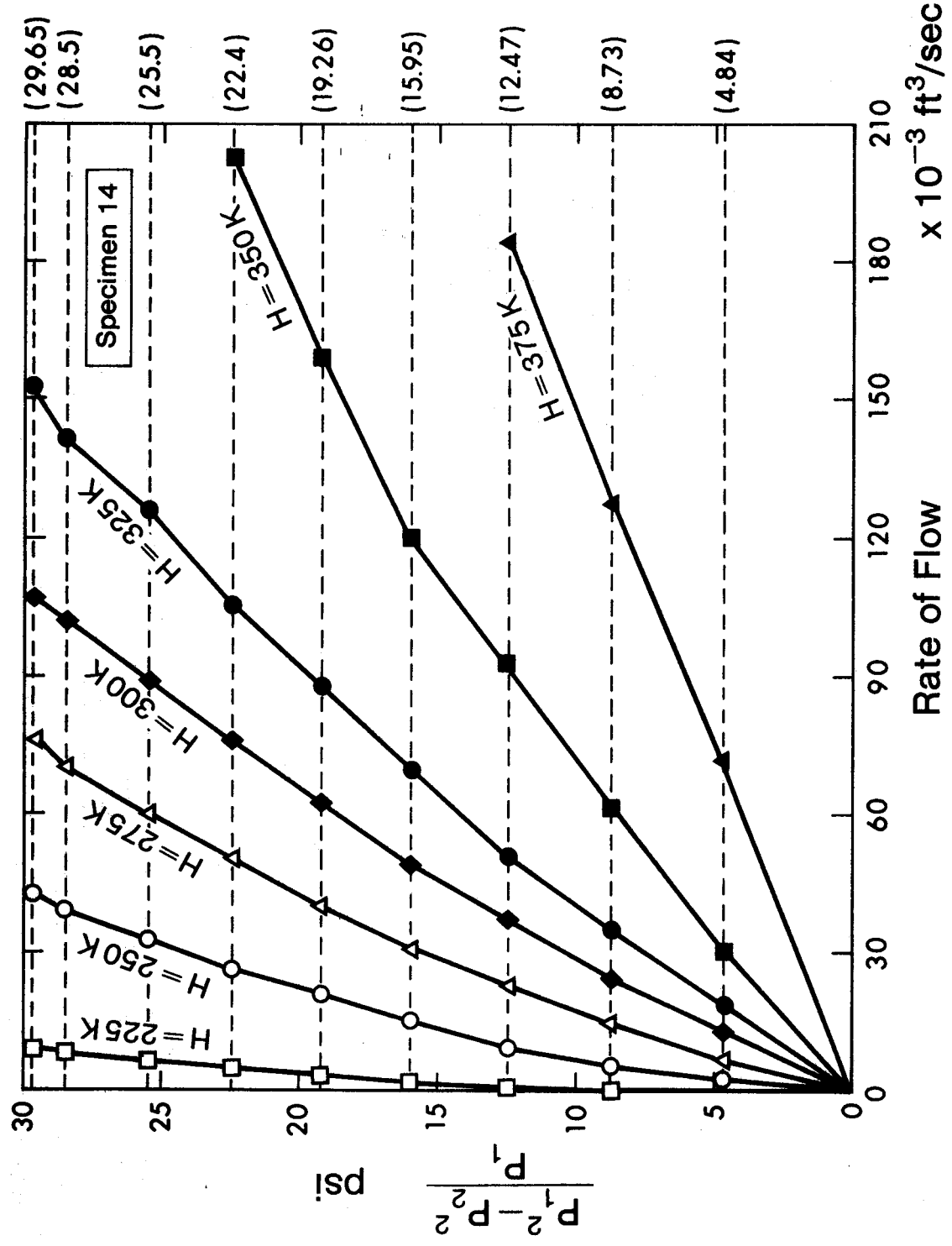

Fig. 6.1 Flow Rate - Pressure Gradient Relationship for Segment 14

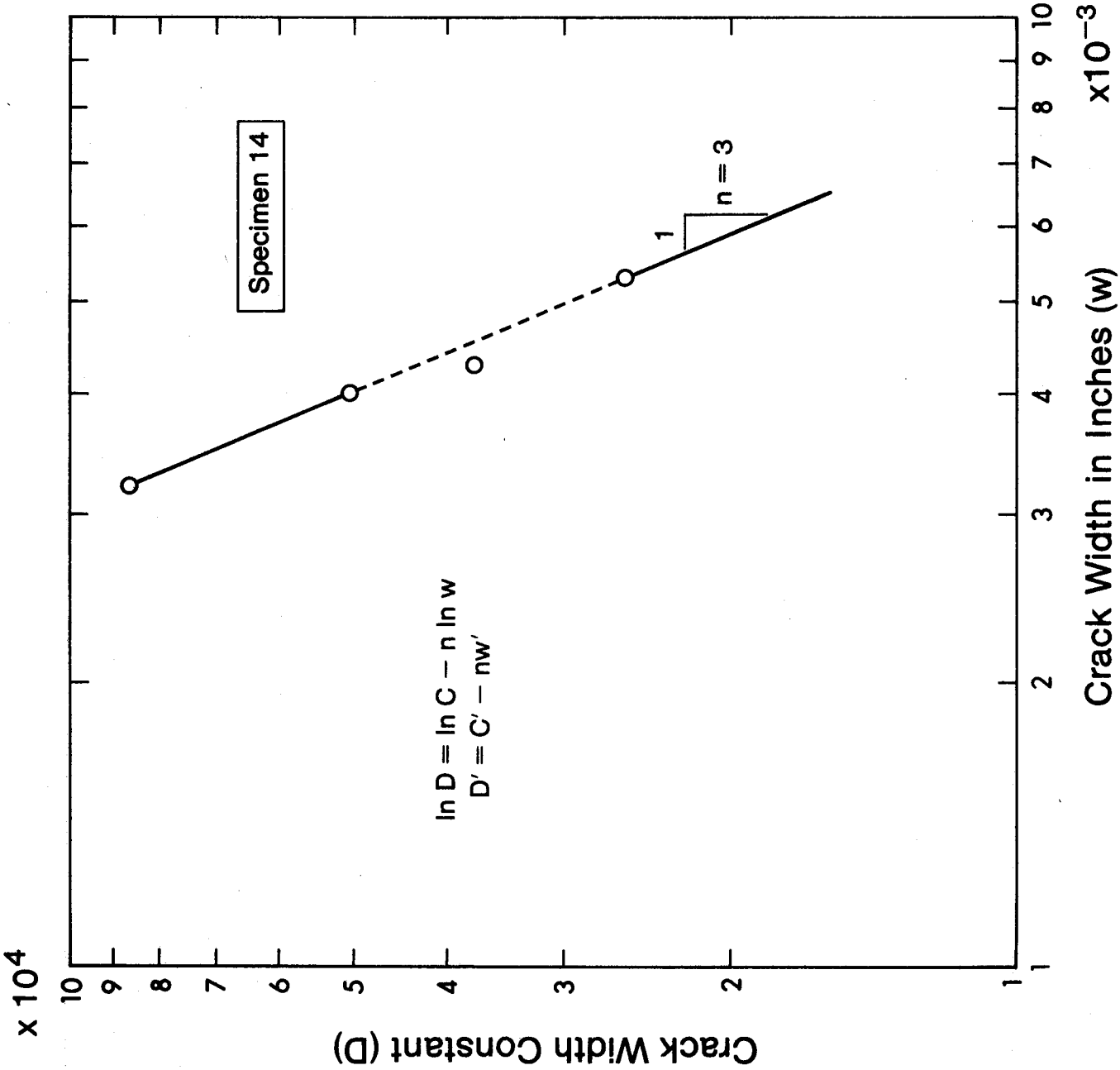

Fig. 6.2 Relationship between D and Crack Width, Segment 14

APPENDIX A

Loads and Strain Data

SPECIMEN 10, FACE A

LOADS AND STRAINS FROM EMBEDDED STEEL GAGES

VERTICAL DIRECTION

H. LOAD (KIPS)	V. LOAD (KIPS)	EMBEDDED STEEL STRAIN 1	2	3
0.5000E+01	0.5119E+01	0.0	0.0	0.0
0.1770E+02	0.2521E+02	0.1603E-04	0.1786E-04	0.2763E-04
0.2940E+02	0.5031E+02	0.3567E-04	0.3039E-04	0.6586E-04
0.4265E+02	0.7524E+02	0.5733E-04	0.5353E-04	0.1148E-03
0.5502E+02	0.1006E+03	0.8343E-04	0.7519E-04	0.1678E-03
0.6741E+02	0.1260E+03	0.1139E-03	0.9877E-04	0.2259E-03
0.8040E+02	0.1508E+03	0.1466E-03	0.1224E-03	0.2946E-03
0.9259E+02	0.1759E+03	0.1827E-03	0.1554E-03	0.3647E-03
0.1055E+03	0.2011E+03	0.2205E-03	0.1780E-03	0.4408E-03
0.1183E+03	0.2259E+03	0.2628E-03	0.2129E-03	0.5292E-03
0.1303E+03	0.2506E+03	0.3116E-03	0.2494E-03	0.6224E-03
0.1427E+03	0.2759E+03	0.3674E-03	0.2886E-03	0.7166E-03
0.1555E+03	0.3009E+03	0.4406E-03	0.3460E-03	0.8354E-03
0.1680E+03	0.3292E+03	0.6142E-03	0.7430E-03	0.1055E-02
0.1839E+03	0.3507E+03	0.7386E-03	0.9544E-03	0.1174E-02
0.1810E+03	0.3507E+03	0.8036E-03	0.1098E-02	0.1317E-02
0.1930E+03	0.3756E+03	0.9041E-03	0.1236E-02	0.1393E-02
0.2071E+03	0.4005E+03	0.1154E-02	0.1532E-02	0.1644E-02
0.2312E+03	0.4513E+03	0.1791E-02	0.2319E-02	0.2080E-02
0.2553E+03	0.5017E+03	0.2679E-02	0.3137E-02	0.2624E-02
0.2793E+03	0.5509E+03	0.1399E-01	0.3993E-02	0.3569E-02
0.2874E+03	0.5664E+03	0.1846E-01	0.1781E-01	0.3700E-02
0.3094E+03	0.5667E+03	0.2083E-01	0.1791E-01	0.3720E-02
0.3306E+03	0.5667E+03	0.1955E-01	0.1814E-01	0.3795E-02
0.3548E+03	0.5667E+03	0.1969E-01	0.1833E-01	0.3799E-02
0.3784E+03	0.5667E+03	0.1986E-01	0.1856E-01	0.3665E-02
0.3489E+03	0.5669E+03	0.1995E-01	0.1864E-01	0.3717E-02
0.2943E+03	0.5669E+03	0.1997E-01	0.1866E-01	0.4688E-02
0.2725E+03	0.5664E+03	0.2001E-01	0.1871E-01	0.6425E-02
0.2331E+03	0.4605E+03	0.1923E-01	0.1784E-01	0.7191E-02
0.2083E+03	0.4017E+03	0.1872E-01	0.1734E-01	0.6812E-02
0.1361E+03	0.2603E+03	0.1763E-01	0.1615E-01	0.5880E-02
0.9935E+02	0.2009E+03	0.1746E-01	0.1601E-01	0.5730E-02
0.5221E+02	0.1005E+03	0.1741E-01	0.1586E-01	0.5671E-02
0.4046E+01	0.5170E+01	0.1736E-01	0.1566E-01	0.5639E-02

SPECIMEN 10, FACE A

LOADS AND STRAINS FROM EMBEDDED STEEL GAGES

HORIZONTAL DIRECTION

H. LOAD (KIPS)	V. LOAD (KIPS)	EMBEDDED STEEL STRAIN 4	5	6
0.5000E+01	0.5119E+01	0.0	0.0	0.0
0.1770E+02	0.2521E+02	0.1436E-04	0.5920E-05	0.1811E-04
0.2940E+02	0.5031E+02	0.2970E-04	0.1855E-04	0.3952E-04
0.4265E+02	0.7524E+02	0.4939E-04	0.3676E-04	0.4445E-04
0.5502E+02	0.1006E+03	0.6419E-04	0.5175E-04	0.6167E-04
0.6741E+02	0.1260E+03	0.8180E-04	0.6818E-04	0.8491E-04
0.8040E+02	0.1508E+03	0.1027E-03	0.8856E-04	0.1242E-03
0.9259E+02	0.1759E+03	0.1243E-03	0.1109E-03	0.2118E-03
0.1055E+03	0.2011E+03	0.1504E-03	0.1381E-03	0.5727E-03
0.1183E+03	0.2259E+03	0.1840E-03	0.1730E-03	0.7261E-03
0.1303E+03	0.2508E+03	0.2674E-03	0.2043E-03	0.8595E-03
0.1427E+03	0.2759E+03	0.5813E-03	0.2420E-03	0.9602E-03
0.1555E+03	0.3009E+03	0.7268E-03	0.2975E-03	0.1072E-02
0.1680E+03	0.3292E+03	0.9915E-03	0.5140E-03	0.1207E-02
0.1839E+03	0.3507E+03	0.1107E-02	0.7672E-03	0.1255E-02
0.1810E+03	0.3507E+03	0.1185E-02	0.9015E-03	0.1192E-02
0.1930E+03	0.3756E+03	0.1239E-02	0.9837E-03	0.1224E-02
0.2071E+03	0.4005E+03	0.1380E-02	0.1193E-02	0.1289E-02
0.2312E+03	0.4513E+03	0.1601E-02	0.1622E-02	0.1393E-02
0.2553E+03	0.5017E+03	0.1678E-02	0.1965E-02	0.1572E-02
0.2793E+03	0.5509E+03	0.1835E-02	0.2228E-02	0.1708E-02
0.2874E+03	0.5664E+03	0.1973E-02	0.2417E-02	0.1780E-02
0.3094E+03	0.5667E+03	0.2102E-02	0.2553E-02	0.1939E-02
0.3306E+03	0.5667E+03	0.2355E-02	0.2935E-02	0.2191E-02
0.3548E+03	0.5667E+03	0.2404E-02	0.1479E-01	0.2234E-02
0.3784E+03	0.5667E+03	0.2488E-02	0.1544E-01	0.2304E-02
0.3489E+03	0.5669E+03	0.2264E-02	0.1523E-01	0.2089E-02
0.2943E+03	0.5669E+03	0.1781E-02	0.1472E-01	0.1602E-02
0.2725E+03	0.5664E+03	0.1579E-02	0.1450E-01	0.1399E-02
0.2331E+03	0.4605E+03	0.1214E-02	0.1406E-01	0.1024E-02
0.2083E+03	0.4017E+03	0.1015E-02	0.1380E-01	0.8210E-03
0.1361E+03	0.2603E+03	0.5101E-03	0.1310E-01	0.3340E-03
0.9935E+02	0.2009E+03	0.4667E-03	0.1302E-01	0.3063E-03
0.5221E+02	0.1005E+03	0.2227E-03	0.1268E-01	0.3138E-03
0.4046E+01	0.5170E+01	-0.1351E-03	0.1201E-01	0.2998E-03

SPECIMEN 10, FACE B

LOADS AND STRAINS FROM EMBEDDED STEEL GAGES

VERTICAL DIRECTION

H. LOAD (KIPS)	V. LOAD (KIPS)	EMBEDDED STEEL STRAIN 7	8	9
0.5000E+01	0.5119E+01	0.0	0.0	0.0
0.1770E+02	0.2521E+02	0.1463E-04	0.1347E-04	0.1391E-04
0.2940E+02	0.5031E+02	0.2530E-04	0.3666E-04	0.3473E-04
0.4265E+02	0.7524E+02	0.3558E-04	0.5294E-04	0.5827E-04
0.5502E+02	0.1006E+03	0.4902E-04	0.6991E-04	0.8170E-04
0.6741E+02	0.1260E+03	0.5930E-04	0.8767E-04	0.1083E-03
0.8040E+02	0.1508E+03	0.7314E-04	0.1042E-03	0.1395E-03
0.9259E+02	0.1759E+03	0.8817E-04	0.1221E-03	0.1744E-03
0.1055E+03	0.2011E+03	0.1028E-03	0.1400E-03	0.2290E-03
0.1183E+03	0.2259E+03	0.1218E-03	0.1617E-03	0.3304E-03
0.1303E+03	0.2508E+03	0.1558E-03	0.1817E-03	0.5025E-03
0.1427E+03	0.2759E+03	0.2507E-03	0.2004E-03	0.6028E-03
0.1555E+03	0.3009E+03	0.6200E-03	0.2214E-03	0.8317E-03
0.1680E+03	0.3292E+03	0.9083E-03	0.1201E-02	0.1085E-02
0.1839E+03	0.3507E+03	0.1069E-02	0.1521E-02	0.1306E-02
0.1810E+03	0.3507E+03	0.1174E-02	0.1625E-02	0.1381E-02
0.1930E+03	0.3756E+03	0.1287E-02	0.1879E-02	0.1502E-02
0.2071E+03	0.4005E+03	0.1452E-02	0.2179E-02	0.1670E-02
0.2312E+03	0.4513E+03	0.1802E-02	0.2834E-02	0.1916E-02
0.2553E+03	0.5017E+03	0.2310E-02	0.1372E-01	0.2066E-02
0.2793E+03	0.5509E+03	0.2722E-02	0.1746E-01	0.2312E-02
0.2874E+03	0.5664E+03	0.1609E-01	0.2110E-01	0.1491E-01
0.3094E+03	0.5667E+03	0.1693E-01	0.2186E-01	0.1554E-01
0.3306E+03	0.5667E+03	0.1768E-01	0.2230E-01	0.1596E-01
0.3548E+03	0.5667E+03	0.1838E-01	0.2271E-01	0.1631E-01
0.3784E+03	0.5667E+03	0.1896E-01	0.2313E-01	0.1641E-01
0.3489E+03	0.5669E+03	0.1926E-01	0.2326E-01	0.1639E-01
0.2943E+03	0.5669E+03	0.1943E-01	0.2336E-01	0.1637E-01
0.2725E+03	0.5664E+03	0.1955E-01	0.2346E-01	0.1637E-01
0.2331E+03	0.4605E+03	0.1881E-01	0.2248E-01	0.1560E-01
0.2083E+03	0.4017E+03	0.1830E-01	0.2190E-01	0.1509E-01
0.1361E+03	0.2603E+03	0.1711E-01	0.2046E-01	0.1386E-01
0.9935E+02	0.2009E+03	0.1693E-01	0.2019E-01	0.1368E-01
0.5221E+02	0.1005E+03	0.1693E-01	0.2013E-01	0.1357E-01
0.4046E+01	0.5170E+01	0.1690E-01	0.2000E-01	0.1344E-01

SPECIMEN 10, FACE B

LOADS AND STRAINS FROM EMBEDDED STEEL GAGES

HORIZONTAL DIRECTION

H. LOAD (KIPS)	V. LOAD (KIPS)	EMBEDDED STEEL STRAIN 10	11	12
0.5000E+01	0.5119E+01	0.0	0.0	0.0
0.1770E+02	0.2521E+02	0.4243E-05	-0.2319E-05	0.7943E-05
0.2940E+02	0.5031E+02	0.1056E-04	-0.6907E-06	0.1446E-04
0.4265E+02	0.7524E+02	0.1978E-04	-0.3898E-05	0.1677E-04
0.5502E+02	0.1006E+03	0.2432E-04	-0.5158E-05	0.2126E-04
0.6741E+02	0.1260E+03	0.2891E-04	-0.2121E-05	0.2625E-04
0.8040E+02	0.1508E+03	0.3330E-04	-0.4934E-07	0.3222E-04
0.9259E+02	0.1759E+03	0.3750E-04	0.1875E-05	0.3883E-04
0.1055E+03	0.2011E+03	0.4297E-04	-0.1776E-05	0.5022E-04
0.1183E+03	0.2259E+03	0.5077E-04	-0.1431E-05	0.6113E-04
0.1303E+03	0.2508E+03	0.5886E-04	0.6414E-05	0.7356E-04
0.1427E+03	0.2759E+03	0.6882E-04	0.1145E-04	0.8580E-04
0.1555E+03	0.3009E+03	0.8520E-04	0.9177E-05	0.1073E-03
0.1680E+03	0.3292E+03	0.1585E-03	0.6868E-04	0.2932E-03
0.1839E+03	0.3507E+03	0.2797E-03	0.1916E-03	0.5695E-03
0.1810E+03	0.3507E+03	0.3649E-03	0.1669E-03	0.5833E-03
0.1930E+03	0.3756E+03	0.4495E-03	0.2364E-03	0.7471E-03
0.2071E+03	0.4005E+03	0.6552E-03	0.4167E-03	0.9620E-03
0.2312E+03	0.4513E+03	0.1044E-02	0.7870E-03	0.1264E-02
0.2553E+03	0.5017E+03	0.1373E-02	0.1053E-02	0.1529E-02
0.2793E+03	0.5509E+03	0.1707E-02	0.1393E-02	0.1871E-02
0.2874E+03	0.5664E+03	0.1929E-02	0.2019E-02	0.2159E-02
0.3094E+03	0.5667E+03	0.2083E-02	0.2270E-02	0.2349E-02
0.3306E+03	0.5667E+03	0.2417E-02	0.2604E-02	0.2569E-02
0.3548E+03	0.5667E+03	0.2543E-02	0.3073E-02	0.2432E-02
0.3784E+03	0.5667E+03	0.2608E-02	0.4399E-02	0.3236E-02
0.3489E+03	0.5669E+03	0.2431E-02	0.4427E-02	0.3154E-02
0.2943E+03	0.5669E+03	0.2022E-02	0.4061E-02	0.2750E-02
0.2725E+03	0.5664E+03	0.1848E-02	0.3905E-02	0.2574E-02
0.2331E+03	0.4605E+03	0.1507E-02	0.3506E-02	0.2209E-02
0.2083E+03	0.4017E+03	0.1336E-02	0.3278E-02	0.2009E-02
0.1361E+03	0.2603E+03	0.9578E-03	0.2798E-02	0.1550E-02
0.9935E+02	0.2009E+03	0.9178E-03	0.2732E-02	0.1524E-02
0.5221E+02	0.1005E+03	0.8588E-03	0.2610E-02	0.1500E-02
0.4046E+01	0.5170E+01	0.7052E-03	0.2383E-02	0.1423E-02

SPECIMEN 10

LOADS AND AVERAGE STRAINS FROM EMBEDDED STEEL GAGES

H. LOAD (KIPS)	V. LOAD (KIPS)	AVG. HOR. FACE A	AVG. HOR. FACE B	AVG. HOR. BOTH FACES	AVG. VERT. FACE A	AVG. VERT. FACE B	AVG. VERT. BOTH FACES
0.5000E+01	0.5119E+01	0.0	0.0	0.0	0.0	0.0	0.0
0.1770E+02	0.2521E+02	0.1014E-04	0.3289E-05	0.6714E-05	0.2051E-04	0.1400E-04	0.1726E-04
0.2940E+02	0.5031E+02	0.2413E-04	0.8108E-05	0.1612E-04	0.4398E-04	0.3223E-04	0.3810E-04
0.4265E+02	0.7524E+02	0.4307E-04	0.1089E-04	0.2698E-04	0.7522E-04	0.4893E-04	0.6208E-04
0.5502E+02	0.1006E+03	0.5797E-04	0.1414E-04	0.3606E-04	0.1088E-03	0.6688E-04	0.8785E-04
0.6741E+02	0.1260E+03	0.7499E-04	0.1768E-04	0.4634E-04	0.1462E-03	0.8511E-04	0.1156E-03
0.8040E+02	0.1508E+03	0.9561E-04	0.2182E-04	0.5872E-04	0.1879E-03	0.1056E-03	0.1467E-03
0.9259E+02	0.1759E+03	0.1176E-03	0.2607E-04	0.7183E-04	0.2343E-03	0.1282E-03	0.1812E-03
0.1055E+03	0.2011E+03	0.1443E-03	0.3047E-04	0.8738E-04	0.2798E-03	0.1573E-03	0.2185E-03
0.1193E+03	0.2259E+03	0.1785E-03	0.3682E-04	0.1077E-03	0.3350E-03	0.2046E-03	0.2698E-03
0.1303E+03	0.2508E+03	0.2358E-03	0.4628E-04	0.1411E-03	0.3945E-03	0.2800E-03	0.3372E-03
0.1427E+03	0.2759E+03	0.4116E-03	0.5536E-04	0.2335E-03	0.4576E-03	0.3513E-03	0.4044E-03
0.1555E+03	0.3009E+03	0.5121E-03	0.6723E-04	0.2897E-03	0.5407E-03	0.5577E-03	0.5492E-03
0.1680E+03	0.3292E+03	0.7527E-03	0.1735E-03	0.4631E-03	0.8041E-03	0.1065E-02	0.9345E-03
0.1839E+03	0.3507E+03	0.9371E-03	0.3469E-03	0.6420E-03	0.9556E-03	0.1298E-02	0.1127E-02
0.1810E+03	0.3507E+03	0.1043E-02	0.3717E-03	0.7076E-03	0.1073E-02	0.1393E-02	0.1233E-02
0.1930E+03	0.3756E+03	0.1112E-02	0.4776E-03	0.7946E-03	0.1177E-02	0.1556E-02	0.1367E-02
0.2071E+03	0.4005E+03	0.1286E-02	0.6780E-03	0.9821E-03	0.1443E-02	0.1767E-02	0.1605E-02
0.2312E+03	0.4513E+03	0.1612E-02	0.1032E-02	0.1322E-02	0.2063E-02	0.2184E-02	0.2124E-02
0.2553E+03	0.5017E+03	0.1822E-02	0.1318E-02	0.1570E-02	0.2814E-02	0.6033E-02	0.4423E-02
0.2793E+03	0.5509E+03	0.2032E-02	0.1657E-02	0.1844E-02	0.7184E-02	0.7497E-02	0.7340E-02
0.2874E+03	0.5664E+03	0.2195E-02	0.2036E-02	0.2115E-02	0.1332E-01	0.1736E-01	0.1534E-01
0.3094E+03	0.5667E+03	0.2328E-02	0.2234E-02	0.2281E-02	0.1415E-01	0.1811E-01	0.1613E-01
0.3306E+03	0.5667E+03	0.2645E-02	0.2530E-02	0.2587E-02	0.1383E-01	0.1865E-01	0.1624E-01
0.3548E+03	0.5667E+03	0.8595E-02	0.2683E-02	0.5639E-02	0.1394E-01	0.1913E-01	0.1654E-01
0.3784E+03	0.5667E+03	0.8965E-02	0.3414E-02	0.6190E-02	0.1403E-01	0.1950E-01	0.1676E-01
0.3489E+03	0.5669E+03	0.8748E-02	0.3337E-02	0.6043E-02	0.1410E-01	0.1964E-01	0.1687E-01
0.2943E+03	0.5669E+03	0.8251E-02	0.2945E-02	0.5598E-02	0.1444E-01	0.1972E-01	0.1708E-01
0.2725E+03	0.5664E+03	0.8038E-02	0.2776E-02	0.5407E-02	0.1505E-01	0.1979E-01	0.1742E-01
0.2331E+03	0.4605E+03	0.7637E-02	0.2407E-02	0.5022E-02	0.1475E-01	0.1896E-01	0.1686E-01
0.2083E+03	0.4017E+03	0.7408E-02	0.2207E-02	0.4808E-02	0.1429E-01	0.1843E-01	0.1636E-01
0.1361E+03	0.2503E+03	0.6807E-02	0.1769E-02	0.4288E-02	0.1322E-01	0.1715E-01	0.1518E-01
0.9935E+02	0.2009E+03	0.6745E-02	0.1725E-02	0.4235E-02	0.1306E-01	0.1693E-01	0.1500E-01
0.5221E+02	0.1005E+03	0.6453E-02	0.1656E-02	0.4055E-02	0.1298E-01	0.1687E-01	0.1493E-01
0.4046E+01	0.5170E+01	0.5935E-02	0.1504E-02	0.3720E-02	0.1289E-01	0.1678E-01	0.1483E-01

SPECIMEN 10

LOADS AND STRAINS FROM LINEARLY VARYING DIFFERENTIAL TRANSFORMERS

H. LOAD (KIPS)	V. LOAD (KIPS)	LVDT TOP	LVDT BOTTOM	LVDT WEST	LVDT EAST	AVG. STRAIN TOP - BOTTOM	AVG. STRAIN WEST - EAST
0.5000E+01	0.5119E+01	0.0	0.0	0.0	0.0	0.0	0.0
0.1770E+02	0.2521E+02	0.1531E-04	0.1465E-06	-0.9712E-07	-0.1303E-04	0.7730E-05	-0.6565E-05
0.2940E+02	0.5031E+02	0.4959E-04	0.1235E-04	0.1008E-04	-0.2842E-04	0.3097E-04	-0.9169E-05
0.4265E+02	0.7524E+02	0.6627E-04	0.1497E-04	0.1658E-04	0.1359E-03	0.4062E-04	0.7625E-04
0.5502E+02	0.1006E+03	0.6646E-04	0.2205E-04	0.1666E-04	0.1204E-03	0.4426E-04	0.6853E-04
0.6741E+02	0.1260E+03	0.6837E-04	0.3248E-04	0.3001E-04	0.1033E-03	0.5043E-04	0.6664E-04
0.8040E+02	0.1508E+03	0.7003E-04	0.4250E-04	0.5801E-04	0.8434E-04	0.5626E-04	0.7117E-04
0.9259E+02	0.1759E+03	0.7428E-04	0.5758E-04	0.8723E-04	0.6514E-04	0.6593E-04	0.7618E-04
0.1055E+03	0.2011E+03	0.8993E-04	0.7273E-04	0.1114E-03	0.4264E-04	0.8133E-04	0.7704E-04
0.1183E+03	0.2259E+03	0.1285E-03	0.1025E-03	0.2030E-03	0.1261E-04	0.1155E-03	0.1078E-03
0.1303E+03	0.2508E+03	0.1391E-03	0.1216E-03	0.2059E-03	-0.2277E-04	0.1303E-03	0.9158E-04
0.1427E+03	0.2759E+03	0.1621E-03	0.1499E-03	0.2384E-03	-0.5072E-04	0.1560E-03	0.9382E-04
0.1555E+03	0.3009E+03	0.2004E-03	0.1961E-03	0.2981E-03	-0.1077E-03	0.1983E-03	0.9518E-04
0.1680E+03	0.3292E+03	0.3468E-03	0.3053E-03	0.4840E-03	-0.4220E-03	0.3260E-03	0.3103E-04
0.1839E+03	0.3507E+03	0.5182E-03	0.3786E-03	0.6428E-03	-0.6362E-03	0.4484E-03	0.3329E-05
0.1810E+03	0.3507E+03	0.5941E-03	0.4338E-03	0.8026E-03	-0.7720E-03	0.5140E-03	0.1529E-04
0.1930E+03	0.3756E+03	0.6534E-03	0.4338E-03	0.8012E-03	-0.9268E-03	0.5436E-03	-0.6276E-04
0.2071E+03	0.4005E+03	0.7469E-03	0.5033E-03	0.1043E-02	-0.1204E-02	0.6251E-03	-0.8077E-04
0.2312E+03	0.4513E+03	0.9317E-03	0.6540E-03	0.1511E-02	-0.1648E-02	0.7928E-03	-0.6829E-04
0.2553E+03	0.5017E+03	0.1296E-02	0.8649E-03	0.1788E-02	-0.2123E-02	0.1080E-02	-0.1672E-03
0.2793E+03	0.5509E+03	0.1675E-02	0.1113E-02	0.2858E-02	-0.2573E-02	0.1394E-02	0.1425E-03
0.2674E+03	0.5664E+03	0.2194E-02	0.1292E-02	0.4827E-02	-0.2651E-02	0.1743E-02	0.1088E-02
0.3094E+03	0.5667E+03	0.2314E-02	0.1441E-02	0.5524E-02	-0.2662E-02	0.1878E-02	0.1431E-02
0.3306E+03	0.5667E+03	0.2468E-02	0.1620E-02	0.6399E-02	-0.2787E-02	0.2044E-02	0.1806E-02
0.3548E+03	0.5667E+03	0.2957E-02	0.1873E-02	0.7350E-02	-0.2781E-02	0.2415E-02	0.2284E-02
0.3784E+03	0.5667E+03	0.3678E-02	0.2253E-02	0.8307E-02	-0.2793E-02	0.2966E-02	0.2757E-02
0.3489E+03	0.5669E+03	0.3647E-02	0.2207E-02	0.8717E-02	-0.2794E-02	0.2927E-02	0.2962E-02
0.2943E+03	0.5669E+03	0.3412E-02	0.1993E-02	0.8815E-02	-0.2785E-02	0.2702E-02	0.3015E-02
0.2725E+03	0.5664E+03	0.3317E-02	0.1914E-02	0.8931E-02	-0.2791E-02	0.2616E-02	0.3070E-02
0.2331E+03	0.4605E+03	0.3111E-02	0.1710E-02	0.8414E-02	-0.2782E-02	0.2410E-02	0.2816E-02
0.2083E+03	0.4017E+03	0.3015E-02	0.1617E-02	0.8009E-02	-0.2783E-02	0.2316E-02	0.2613E-02
0.1361E+03	0.2603E+03	0.2727E-02	0.1379E-02	0.7108E-02	-0.2783E-02	0.2053E-02	0.2162E-02
0.9935E+02	0.2009E+03	0.2698E-02	0.1331E-02	0.6921E-02	-0.2782E-02	0.2015E-02	0.2070E-02
0.5221E+02	0.1005E+03	0.2582E-02	0.1265E-02	0.6795E-02	-0.2782E-02	0.1924E-02	0.2006E-02
0.4046E+01	0.5170E+01	0.2365E-02	0.1184E-02	0.6527E-02	-0.2782E-02	0.1775E-02	0.1872E-02

SPECIMEN 14, FACE A

LOADS AND STRAINS FROM EMBEDDED STEEL GAGES

HORIZONTAL DIRECTION

H. LOAD (KIPS)	V. LOAD (KIPS)	EMBEDDED STEEL STRAIN 4	5	6
0.5000E+01	0.0	0.0	0.0	0.0
0.3065E+02	0.0	0.1194E-04	0.6414E-05	0.1806E-04
0.5577E+02	0.0	0.3005E-04	0.2581E-04	0.3631E-04
0.8046E+02	0.0	0.4712E-04	0.4352E-04	0.5339E-04
0.1057E+03	0.0	0.6992E-04	0.6528E-04	-0.7401E-04
0.1304E+03	0.0	0.1020E-03	0.9005E-04	0.9755E-04
0.1563E+03	0.0	0.1448E-03	0.1194E-03	0.1235E-03
0.1817E+03	0.0	0.1968E-03	0.1507E-03	0.1528E-03
0.2068E+03	0.0	0.2593E-03	0.1951E-03	0.1950E-03
0.2305E+03	0.0	0.3527E-03	0.3261E-03	0.8041E-03
0.2312E+03	0.0	0.4419E-03	0.7355E-03	0.8241E-03
0.2553E+03	0.0	0.5074E-03	0.1025E-02	0.9728E-03
0.2545E+03	0.0	0.6080E-03	0.1095E-02	0.1024E-02
0.2800E+03	0.0	0.6833E-03	0.1307E-02	0.1189E-02
0.2811E+03	0.0	0.7492E-03	0.1250E-02	0.1169E-02
0.3062E+03	0.0	0.9634E-03	0.1622E-02	0.1449E-02
0.3062E+03	0.0	0.1032E-02	0.1618E-02	0.1462E-02
0.3301E+03	0.0	0.1260E-02	0.1859E-02	0.1670E-02
0.3304E+03	0.0	0.1262E-02	0.1685E-02	0.1583E-02
0.3554E+03	0.0	0.1528E-02	0.2114E-02	0.1907E-02
0.3551E+03	0.0	0.1585E-02	0.2077E-02	0.1900E-02
0.3804E+03	0.0	0.1771E-02	0.2345E-02	0.2140E-02
0.3812E+03	0.0	0.1829E-02	0.2371E-02	0.2157E-02
0.4046E+03	0.0	0.1976E-02	0.2018E-01	0.2268E-02
0.4046E+03	0.0	0.2013E-02	0.2032E-01	0.2319E-02
0.3511E+03	0.0	0.1739E-02	0.1979E-01	0.1968E-02
0.3065E+03	0.0	0.1420E-02	0.1936E-01	0.1604E-02
0.2559E+03	0.0	0.1047E-02	0.1892E-01	0.1213E-02
0.2062E+03	0.0	0.6932E-03	0.1844E-01	0.8731E-03
0.1536E+03	0.0	0.3692E-03	0.1786E-01	0.5873E-03
0.1013E+03	0.0	0.2210E-03	0.1706E-01	0.3612E-03
0.5787E+02	0.0	0.1464E-03	0.1613E-01	0.1824E-03
0.3381E+01	0.0	0.3479E-04	0.1466E-01	-0.9473E-05

SPECIMEN 14, FACE A

LOADS AND STRAINS FROM EMBEDDED STEEL GAGES

VERTICAL DIRECTION

H. LOAD (KIPS)	V. LOAD (KIPS)	EMBEDDED STEEL STRAIN 1	2	3
0.5000E+01	0.0	0.0	0.0	0.0
0.3065E+02	0.0	-0.6414E-06	0.9868E-07	-0.7894E-06
0.5577E+02	0.0	-0.2122E-05	-0.2960E-06	-0.2072E-05
0.8046E+02	0.0	-0.8191E-05	-0.6710E-05	-0.8635E-05
0.1057E+03	0.0	-0.1031E-04	-0.1081E-04	-0.1179E-04
0.1304E+03	0.0	-0.9079E-05	-0.1268E-04	-0.1056E-04
0.1583E+03	0.0	-0.1085E-04	-0.1786E-04	-0.1367E-04
0.1817E+03	0.0	-0.4687E-05	-0.1757E-04	-0.9079E-05
0.2068E+03	0.0	-0.1234E-05	-0.2467E-04	-0.7056E-05
0.2305E+03	0.0	0.1185E-03	0.2674E-04	0.1687E-04
0.2312E+03	0.0	0.1357E-03	0.5052E-04	0.2748E-04
0.2553E+03	0.0	0.1617E-03	0.4835E-04	0.3434E-04
0.2545E+03	0.0	0.1665E-03	0.3878E-04	0.2640E-04
0.2800E+03	0.0	0.1887E-03	0.3306E-04	0.3044E-04
0.2811E+03	0.0	0.1796E-03	0.2136E-04	0.2023E-04
0.3062E+03	0.0	0.2123E-03	0.2477E-04	0.3232E-04
0.3062E+03	0.0	0.2103E-03	0.2551E-04	0.3015E-04
0.3301E+03	0.0	0.2401E-03	0.2600E-04	0.4140E-04
0.3304E+03	0.0	0.2369E-03	0.1396E-04	0.2354E-04
0.3554E+03	0.0	0.2603E-03	0.1900E-04	0.4732E-04
0.3551E+03	0.0	0.2381E-03	0.2378E-04	0.4870E-04
0.3804E+03	0.0	0.2435E-03	0.2798E-04	0.5299E-04
0.3812E+03	0.0	0.2297E-03	0.1263E-04	0.5008E-04
0.4046E+03	0.0	0.2290E-03	0.2304E-04	0.5506E-04
0.4046E+03	0.0	0.2272E-03	0.1312E-04	0.5255E-04
0.3511E+03	0.0	0.1905E-03	0.2714E-04	0.4485E-04
0.3065E+03	0.0	0.1522E-03	0.4322E-04	0.3474E-04
0.2559E+03	0.0	0.1140E-03	0.5802E-04	0.2324E-04
0.2062E+03	0.0	0.8082E-04	0.6853E-04	0.1382E-04
0.1536E+03	0.0	0.5408E-04	0.7885E-04	0.1248E-04
0.1013E+03	0.0	0.4006E-04	0.8082E-04	-0.2418E-05
0.5787E+02	0.0	0.3686E-04	0.7786E-04	-0.9819E-05
0.3381E+01	0.0	0.4258E-04	0.7746E-04	-0.1071E-04

SPECIMEN 14, FACE B

LOADS AND STRAINS FROM EMBEDDED STEEL GAGES

HORIZONTAL DIRECTION

H. LOAD (KIPS)	V. LOAD (KIPS)	EMBEDDED STEEL STRAIN 10	11	12
0.5000E+01	0.0	0.0	0.0	0.0
0.3065E+02	0.0	0.1732E-04	0.1900E-04	0.2215E-04
0.5577E+02	0.0	0.3646E-04	0.3750E-04	0.4806E-04
0.8046E+02	0.0	0.4825E-04	0.4885E-04	0.7204E-04
0.1057E+03	0.0	0.6636E-04	0.6646E-04	0.1037E-03
0.1304E+03	0.0	0.8807E-04	0.8906E-04	0.1525E-03
0.1583E+03	0.0	0.1085E-03	0.1097E-03	0.2006E-03
0.1817E+03	0.0	0.1376E-03	0.1382E-03	0.2763E-03
0.2068E+03	0.0	0.1532E-03	0.1567E-03	0.3422E-03
0.2305E+03	0.0	0.7834E-03	0.2906E-03	0.4660E-03
0.2312E+03	0.0	0.9380E-03	0.4065E-03	0.5965E-03
0.2553E+03	0.0	0.1084E-02	0.5189E-03	0.6835E-03
0.2545E+03	0.0	0.1184E-02	0.9289E-03	0.8061E-03
0.2800E+03	0.0	0.1360E-02	0.1026E-02	0.8496E-03
0.2811E+03	0.0	0.1612E-02	0.1421E-02	0.1012E-02
0.3062E+03	0.0	0.1623E-02	0.1452E-02	0.1032E-02
0.3062E+03	0.0	0.1744E-02	0.1636E-02	0.1223E-02
0.3301E+03	0.0	0.1882E-02	0.1761E-02	0.1285E-02
0.3304E+03	0.0	0.2193E-02	0.2029E-02	0.1530E-02
0.3554E+03	0.0	0.2190E-02	0.2043E-02	0.1549E-02
0.3551E+03	0.0	0.2111E-02	0.1995E-02	0.1601E-02
0.3804E+03	0.0	0.2288E-02	0.2141E-02	0.1670E-02
0.3812E+03	0.0	0.2127E-02	0.2059E-02	0.1651E-02
0.4046E+03	0.0	0.2292E-02	0.2127E-02	0.1676E-02
0.4046E+03	0.0	0.2879E-02	0.2107E-02	0.1669E-02
0.3511E+03	0.0	0.2472E-02	0.1779E-02	0.1495E-02
0.3065E+03	0.0	0.2084E-02	0.1460E-02	0.1279E-02
0.2559E+03	0.0	0.1682E-02	0.1119E-02	0.9686E-03
0.2062E+03	0.0	0.1291E-02	0.7812E-03	0.5923E-03
0.1536E+03	0.0	0.9037E-03	0.5174E-03	0.3332E-03
0.1013E+03	0.0	0.5559E-03	0.3520E-03	0.2791E-03
0.5787E+02	0.0	0.2144E-03	0.1925E-03	0.1577E-03
0.3391E+01	0.0	-0.2332E-03	-0.1362E-04	-0.2207E-03

SPECIMEN 14, FACE B

LOADS AND STRAINS FROM EMBEDDED STEEL GAGES

VERTICAL DIRECTION

H. LOAD (KIPS)	V. LOAD (KIPS)	EMBEDDED STEEL STRAIN 7	8	9
0.5000E+01	0.0	0.0	0.0	0.0
0.3065E+02	0.0	-0.7697E-05	-0.1085E-05	-0.1480E-06
0.5577E+02	0.0	-0.8931E-05	-0.2270E-05	-0.5427E-06
0.8046E+02	0.0	-0.2107E-04	-0.1480E-04	0.5921E-06
0.1057E+03	0.0	-0.2502E-04	-0.1840E-04	-0.1110E-04
0.1304E+03	0.0	-0.2581E-04	-0.1895E-04	-0.1179E-04
0.1583E+03	0.0	-0.3271E-04	-0.2615E-04	-0.1510E-04
0.1817E+03	0.0	-0.3182E-04	-0.2561E-04	-0.9671E-05
0.2068E+03	0.0	-0.3696E-04	-0.3044E-04	-0.1135E-04
0.2305E+03	0.0	-0.4985E-04	-0.7258E-04	-0.8886E-04
0.2312E+03	0.0	-0.3261E-04	-0.6686E-04	-0.8136E-04
0.2553E+03	0.0	-0.1426E-04	-0.5689E-04	-0.1150E-03
0.2545E+03	0.0	-0.3484E-05	-0.5955E-04	-0.1247E-03
0.2800E+03	0.0	0.3355E-05	-0.6834E-04	-0.1546E-03
0.2811E+03	0.0	0.1855E-04	-0.4761E-04	-0.1699E-03
0.3062E+03	0.0	0.1145E-04	-0.5561E-04	-0.1742E-03
0.3062E+03	0.0	0.1416E-04	-0.4228E-04	-0.1667E-03
0.3301E+03	0.0	0.2393E-04	-0.4317E-04	-0.1811E-03
0.3304E+03	0.0	0.4525E-04	-0.1702E-04	-0.1864E-03
0.3554E+03	0.0	0.3612E-04	-0.2299E-04	-0.1833E-03
0.3551E+03	0.0	0.2605E-04	-0.6217E-05	-0.2706E-03
0.3804E+03	0.0	0.2738E-04	-0.1939E-04	-0.3142E-03
0.3812E+03	0.0	0.2502E-04	0.7352E-05	-0.3996E-03
0.4046E+03	0.0	0.4164E-04	0.1446E-04	-0.3854E-03
0.4046E+03	0.0	0.4100E-04	0.3084E-04	-0.3623E-03
0.3511E+03	0.0	0.2684E-04	0.5077E-04	-0.3073E-03
0.3065E+03	0.0	0.1219E-04	0.5635E-04	-0.2658E-03
0.2559E+03	0.0	0.2220E-05	0.5798E-04	-0.2253E-03
0.2062E+03	0.0	-0.5921E-05	0.5645E-04	-0.1895E-03
0.1536E+03	0.0	-0.1520E-04	0.5600E-04	-0.1619E-03
0.1013E+03	0.0	-0.2408E-04	0.5403E-04	-0.1397E-03
0.5787E+02	0.0	-0.2852E-04	0.5447E-04	-0.1179E-03
0.3381E+01	0.0	-0.2339E-04	0.5378E-04	-0.9651E-04

SPECIMEN 14

LOADS AND AVERAGE STRAINS FROM EMBEDDED STEEL GAGES

H. LOAD (KIPS)	V. LOAD (KIPS)	AVG. HOR. FACE A	AVG. HOR. FACE B	AVG. HOR. BOTH FACES	AVG. VERT. FACE A	AVG. VERT. FACE B	AVG. VERT. BOTH FACES
0.5000E+01	0.0	0.0	0.0	0.0	0.0	0.0	0.0
0.3065E+02	0.0	0.1214E-04	0.1949E-04	0.1581E-04	-0.4441E-06	-0.2977E-05	-0.1710E-05
0.5577E+02	0.0	0.3072E-04	0.4067E-04	0.3570E-04	-0.1497E-05	-0.3914E-05	-0.2706E-05
0.8046E+02	0.0	0.4801E-04	0.5638E-04	0.5219E-04	-0.7845E-05	-0.1176E-04	-0.9802E-05
0.1057E+03	0.0	0.6973E-04	0.7883E-04	0.7428E-04	-0.1097E-04	-0.1317E-04	-0.1457E-04
0.1304E+03	0.0	0.9654E-04	0.1099E-03	0.1032E-03	-0.1077E-04	-0.1885E-04	-0.1481E-04
0.1583E+03	0.0	0.1292E-03	0.1396E-03	0.1344E-03	-0.1413E-04	-0.2465E-04	-0.1939E-04
0.1817E+03	0.0	0.1668E-03	0.1840E-03	0.1754E-03	-0.1044E-04	-0.2237E-04	-0.1641E-04
0.2068E+03	0.0	0.2165E-03	0.2173E-03	0.2169E-03	-0.1099E-04	-0.2625E-04	-0.1862E-04
0.2305E+03	0.0	0.4943E-03	0.5133E-03	0.5038E-03	0.5403E-04	-0.7010E-04	-0.8034E-05
0.2312E+03	0.0	0.6672E-03	0.6470E-03	0.6571E-03	0.7123E-04	-0.6028E-04	0.5477E-05
0.2553E+03	0.0	0.8351E-03	0.7622E-03	0.7987E-03	0.8148E-04	-0.6205E-04	0.9712E-05
0.2545E+03	0.0	0.9092E-03	0.9731E-03	0.9411E-03	0.7722E-04	-0.6256E-04	0.7327E-05
0.2800E+03	0.0	0.1060E-02	0.1079E-02	0.1069E-02	0.8406E-04	-0.7320E-04	0.5427E-05
0.2811E+03	0.0	0.1056E-02	0.1349E-02	0.1203E-02	0.7375E-04	-0.6633E-04	0.3709E-05
0.3062E+03	0.0	0.1345E-02	0.1369E-02	0.1357E-02	0.8978E-04	-0.7279E-04	0.8495E-05
0.3062E+03	0.0	0.1370E-02	0.1534E-02	0.1452E-02	0.8867E-04	-0.6495E-04	0.1186E-04
0.3301E+03	0.0	0.1596E-02	0.1642E-02	0.1619E-02	0.1025E-03	-0.6677E-04	0.1786E-04
0.3304E+03	0.0	0.1510E-02	0.1917E-02	0.1713E-02	0.9146E-04	-0.5273E-04	0.1937E-04
0.3554E+03	0.0	0.1850E-02	0.1927E-02	0.1888E-02	0.1089E-03	-0.5673E-04	0.2607E-04
0.3551E+03	0.0	0.1854E-02	0.1903E-02	0.1878E-02	0.1035E-03	-0.8358E-04	0.9975E-05
0.3804E+03	0.0	0.2085E-02	0.2033E-02	0.2059E-02	0.1082E-03	-0.1021E-03	0.3034E-05
0.3812E+03	0.0	0.2119E-02	0.1945E-02	0.2032E-02	0.9748E-04	-0.1224E-03	-0.1247E-04
0.4046E+03	0.0	0.8140E-02	0.2032E-02	0.5086E-02	0.1024E-03	-0.1098E-03	-0.3700E-05
0.4046E+03	0.0	0.8218E-02	0.2218E-02	0.5218E-02	0.9761E-04	-0.9681E-04	0.4020E-06
0.3511E+03	0.0	0.7831E-02	0.1915E-02	0.4873E-02	0.8748E-04	-0.7656E-04	0.5460E-05
0.3065E+03	0.0	0.7460E-02	0.1608E-02	0.4534E-02	0.7671E-04	-0.6575E-04	0.5477E-05
0.2559E+03	0.0	0.7061E-02	0.1257E-02	0.4159E-02	0.6508E-04	-0.5505E-04	0.5016E-05
0.2062E+03	0.0	0.6667E-02	0.8881E-03	0.3778E-02	0.5439E-04	-0.4631E-04	0.4038E-05
0.1536E+03	0.0	0.6272E-02	0.5848E-03	0.3429E-02	0.4847E-04	-0.4038E-04	0.4046E-05
0.1013E+03	0.0	0.5880E-02	0.3957E-03	0.3138E-02	0.3949E-04	-0.3658E-04	0.1456E-05
0.5787E+02	0.0	0.5488E-02	0.1882E-03	0.2838E-02	0.3497E-04	-0.3066E-04	0.2155E-05
0.3381E+01	0.0	0.4895E-02	-0.1559E-03	0.2370E-02	0.3645E-04	-0.2204E-04	0.7204E-05

SPECIMEN 14

LOADS AND STRAINS FROM LINEARLY VARYING DIFFERENTIAL TRANSFORMERS

H. LOAD (KIPS)	V. LOAD (KIPS)	LVDT TOP	LVDT BOTTOM	LVDT WEST	LVDT EAST	AVG. STRAIN TOP - BOTTOM	AVG. STRAIN WEST - EAST
0.5000E+01	0.0	0.0	0.0	0.0	0.0	0.0	0.0
0.3065E+02	0.0	-0.1295E-06	-0.9343E-04	0.0	0.2457E-06	-0.4678E-04	0.1229E-06
0.5577E+02	0.0	-0.2590E-06	-0.9979E-04	0.6990E-07	0.4353E-06	-0.5002E-04	0.2526E-06
0.8046E+02	0.0	0.1418E-04	-0.1047E-03	-0.2399E-04	0.1555E-04	-0.4525E-04	-0.4222E-05
0.1057E+03	0.0	0.2059E-04	-0.9294E-04	-0.2421E-04	0.1540E-04	-0.3617E-04	-0.4402E-05
0.1304E+03	0.0	0.3354E-04	-0.4119E-04	-0.3690E-05	0.9590E-05	-0.3810E-05	0.2950E-05
0.1552E+03	0.0	0.3921E-04	-0.6505E-04	-0.3756E-05	0.9253E-05	-0.1292E-04	0.2748E-05
0.1817E+03	0.0	0.5925E-04	-0.7742E-04	-0.2198E-04	0.1065E-04	-0.9088E-05	-0.2664E-05
0.2068E+03	0.0	0.5902E-04	-0.1339E-03	-0.1809E-04	0.2213E-04	-0.3742E-04	0.2023E-05
0.2305E+03	0.0	0.2384E-03	-0.1102E-03	0.6265E-05	0.7569E-04	0.6409E-04	0.4098E-04
0.2312E+03	0.0	0.2797E-03	0.1688E-03	0.3178E-04	0.1140E-03	0.2243E-03	0.7291E-04
0.2553E+03	0.0	0.4977E-03	0.1595E-03	0.4286E-04	0.1207E-03	0.3286E-03	0.8180E-04
0.2545E+03	0.0	0.5774E-03	0.4873E-03	0.4054E-04	0.1048E-03	0.5324E-03	0.7265E-04
0.2800E+03	0.0	0.6567E-03	0.4661E-03	0.4693E-04	0.1198E-03	0.5614E-03	0.8338E-04
0.2811E+03	0.0	0.7996E-03	-0.2605E-03	0.1292E-04	0.2510E-03	0.2696E-03	0.1320E-03
0.3062E+03	0.0	0.9633E-03	0.6622E-03	0.5055E-04	0.1081E-03	0.8127E-03	0.7932E-04
0.3062E+03	0.0	0.1079E-02	0.4793E-03	0.3283E-04	0.1402E-03	0.7791E-03	0.8649E-04
0.3301E+03	0.0	0.1189E-02	0.7832E-03	0.5107E-04	0.1128E-03	0.9862E-03	0.8194E-04
0.3304E+03	0.0	0.1323E-02	-0.1320E-03	0.1081E-04	0.3069E-03	0.5955E-03	0.1589E-03
0.3554E+03	0.0	0.1429E-02	0.8290E-03	0.8268E-04	0.1160E-03	0.1129E-02	0.9936E-04
0.3551E+03	0.0	0.1684E-02	0.9286E-03	0.9551E-04	0.1234E-03	0.1307E-02	0.1094E-03
0.3804E+03	0.0	0.1984E-02	0.9018E-03	0.9585E-04	0.1234E-03	0.1443E-02	0.1096E-03
0.3812E+03	0.0	0.2282E-02	0.9751E-03	0.1120E-03	0.1344E-03	0.1629E-02	0.1232E-03
0.4046E+03	0.0	0.2768E-02	0.1433E-02	0.1336E-03	0.1248E-03	0.2100E-02	0.1292E-03
0.4046E+03	0.0	0.2970E-02	0.1631E-02	0.1685E-03	0.1201E-03	0.2300E-02	0.1443E-03
0.3511E+03	0.0	0.2746E-02	0.1577E-02	0.1688E-03	0.1197E-03	0.2161E-02	0.1442E-03
0.3065E+03	0.0	0.2466E-02	0.1498E-02	0.1608E-03	0.1196E-03	0.1982E-02	0.1402E-03
0.2559E+03	0.0	0.2163E-02	0.1332E-02	0.1535E-03	0.1195E-03	0.1748E-02	0.1365E-03
0.2062E+03	0.0	0.1867E-02	0.1218E-02	0.1432E-03	0.1193E-03	0.1542E-02	0.1313E-03
0.1536E+03	0.0	0.1599E-02	0.1083E-02	0.1327E-03	0.1192E-03	0.1341E-02	0.1260E-03
0.1013E+03	0.0	0.1379E-02	0.1072E-02	0.1280E-03	0.1204E-03	0.1226E-02	0.1242E-03
0.5787E+02	0.0	0.1169E-02	0.1465E-02	0.1281E-03	0.1205E-03	0.1317E-02	0.1243E-03
0.3381E+01	0.0	0.8670E-03	0.1580E-02	0.1279E-03	0.9761E-04	0.1223E-02	0.1127E-03